Chemical Science

ROYAL SOCIETY OF CHEMISTRY

REVIEW

View Article Online
View Journal | View Issue

Cite this: *Chem. Sci.*, 2023, **14**, 1935

Regulation of the Si/Al ratios and Al distributions of zeolites and their impact on properties

Jialiang Li,[a] Mingkun Gao,[a] Wenfu Yan *[a] and Jihong Yu *[ab]

Zeolites are typically a class of crystalline microporous aluminosilicates that are constructed by SiO_4 and AlO_4 tetrahedra. Because of their unique porous structures, strong Brönsted acidity, molecular-level shape selectivity, exchangeable cations, and high thermal/hydrothermal stability, zeolites are widely used as catalysts, adsorbents, and ion-exchangers in industry. The activity, selectivity, and stability/durability of zeolites in applications are closely related to their Si/Al ratios and Al distributions in the framework. In this review, we discussed the basic principles and the state-of-the-art methodologies for regulating the Si/Al ratios and Al distributions of zeolites, including seed-assisted recipe modification, interzeolite transformation, fluoride media, and usage of organic structure-directing agents (OSDAs), *etc.* The conventional and newly developed characterization methods for determining the Si/Al ratios and Al distributions were summarized, which include X-ray fluorescence spectroscopy (XRF), solid state $^{29}Si/^{27}Al$ magic-angle-spinning nuclear magnetic resonance spectroscopy ($^{29}Si/^{27}Al$ MAS NMR), Fourier-transform infrared spectroscopy (FT-IR), *etc.* The impact of Si/Al ratios and Al distributions on the catalysis, adsorption/separation, and ion-exchange performance of zeolites were subsequently demonstrated. Finally, we presented a perspective on the precise control of the Si/Al ratios and Al distributions of zeolites and the corresponding challenges.

Received 31st October 2022
Accepted 27th December 2022

DOI: 10.1039/d2sc06010h

rsc.li/chemical-science

1. Introduction

Zeolites are crystalline microporous solids in which the frameworks are composed of corner-sharing tetrahedral TO_4 units (T = Si, Al, *etc.*), forming periodic one-dimensional (1D) to three-dimensional (3D) channels with an aperture size of typically <2 nm or inter-connected nano-cages.[1,2] Because of their unique porous structures, large specific surface area, molecular-level shape selectivity, tuneable active sites, and high thermal/hydrothermal stability, zeolites are widely used as catalysts,[3–5] adsorbents,[6,7] and detergents.[8,9] The global zeolite market size was valued at USD 12.6 billion in 2021 and is expected to expand at a compound annual growth rate (CAGR) of 6.2% from 2022 to 2030.[10] To date, over 250 types of zeolitic structures have been recognized by the Structure Commission of the International Zeolite Association (IZA-SC).[11] Each three-letter code is assigned to a confirmed zeolite structure. There are about 20 types of industrialized zeolites including **MFI**, **MOR**, **FAU**, ***BEA**, **MWW**, **LTA**, **FER**, **CHA**, *etc.*[12]

The pure siliceous zeolite structure built of only SiO_4 tetrahedra possesses a neutral framework. The isomorphous substitution of a Si^{4+} by an Al^{3+} generates a negative charge which needs to be compensated by a cation adjacent to the connected oxygen.[3,13,14] Brönsted acidity is thus obtained when the compensating cation is the proton. The strength of Brönsted acidity mainly depends on first the concentration and then the local environment of the AlO_4 tetrahedron, corresponding to the Si/Al ratios and the Al distributions of the framework, respectively. Because of the intrinsic affinity of protons to water and the non-negligible difference in the stabilities between Si–O and Al–O bonds, the concentration and distribution of Al atoms will affect the hydrophilicity/hydrophobicity and stability of zeolites.[15–20] Typically, Y zeolite (**FAU**-type) synthesized with a conventional template-free route usually has Si/Al ratios of <3 and suffers from poor hydrothermal stability during catalysis.[21,22] Therefore, high-silica Y zeolite was either synthesized *via* utilization of organic structure-directing agents (OSDAs)[23,24] or prepared by dealumination of low silica Y zeolite *via* steam treatment.[25] The dealuminated Y zeolite (denoted as ultra-stable Y, USY) exhibited higher hydrothermal stability and good catalytic performance in fluid catalytic cracking (FCC). As for the impacts of Al distributions, for example, the preferential location of Al atoms in the narrow straight/sinusoidal channels of ZSM-5 catalysts would suppress the aromatic-based cycle and facilitate the olefin-based cycle in the methanol-to-olefins (MTO) reaction, which would increase the olefin selectivity (*e.g.*, propylene) and the catalyst lifetime.[26–29] Furthermore, the distributions of Al atoms of zeolites refer to three aspects: (i) the location of Al atoms at/within the individual crystallographically

[a]*State Key Laboratory of Inorganic Synthesis and Preparative Chemistry, College of Chemistry, Jilin University, 2699 Qianjin Street, Changchun 130012, China. E-mail: jihong@jlu.edu.cn; yanw@jlu.edu.cn*

[b]*International Center of Future Science, Jilin University, 2699 Qianjin Street, Changchun 130012, China*

distinguishable framework T sites; (ii) the relation of two or more Al atoms in the framework, including their distances and the possibility of cooperation; and (iii) the location of Al atoms at specific positions such as the intersections of the channels.

To get an appropriate Brönsted acidity, it is often necessary to break the limitation of the current Si/Al ratios of zeolites, which is much more difficult for specific zeotype frameworks such as Y zeolite.[23,30] Meanwhile, regulating the Al distributions of zeolites is very challenging because of the randomly located Al atoms within the equivalent crystallographically distinguishable framework T sites in zeolites and the difficulty in determining their spatial distribution.[31] Developing an ingenious strategy for the synthesis and new methods for analysing Si/Al ratios and Al distributions is crucially needed.

There have been several excellent reviews regarding the acid sites or Al distributions of zeolites.[32–35] However, they tend to be organized on the basis of the generation of acidity and the corresponding applications. Therefore, a comprehensive review throughout the process of regulating and determining the Si/Al ratios and Al distributions of zeolites and on the corresponding impacts on the performance of zeolites is very helpful in establishing the relationship between the Si/Al ratios and Al distributions of zeolites and their functionalities.

In this review, we comprehensively surveyed the latest studies related to the regulation of the Si/Al ratios and Al distributions of zeolites including the synthetic strategies and methodologies, mechanisms, characterization techniques, and impacts on the catalysis, adsorption/separation, and ion-exchange performance. However, due to the unclear synthesis mechanism of zeolites, the precise control of the Si/Al ratios and Al distributions of zeolites remains challenging. In this review, the insights and keys for regulating Si/Al ratios and Al distributions are presented. We hope that this review will be helpful to the chemists in academic and industrial fields working on the synthesis, modification, characterization, and applications of zeolites.

2. Regulation of the Si/Al ratios of zeolites

During the formation of aluminosilicate zeolite, it is well accepted that the long-range ordering of the framework is formed by the assembly of aluminosilicate oligomers with specific structures and Si/Al ratios, which determine the Si/Al ratios of the framework of a zeolite.[36–38]

Basically, tuning the Si/Al ratios of zeolites can be achieved by modifying the gel chemistry (mostly Si/Al ratios) of the synthetic mixture and the "post-treatment" of synthesized zeolite crystals of zeolites, which correspond to the "bottom-up" and "top-down" strategies (Fig. 1), respectively. In the terminology of zeolites, "high-silica" and "Si-rich" usually refer to the high Si/Al ratios of a zeolite, while "low-silica" and "Al-rich" usually refer to the low Si/Al ratios of a zeolite. However, the classification of Si/Al ratios into "Si-rich" or "Al-rich" is just applicable to the given zeolite. For example, the typical Si/Al ratios of Beta zeolite synthesized without organic structure-directing agents (OSDAs) in a basic medium often range from 4 to 6.[39–41] For Beta (***BEA**) zeolite," Al-rich" usually refers to Si/Al ratios of <5 and "high-silica" usually refers to Si/Al ratios of >10.[42,43] For Y zeolite (**FAU**), "high-silica" corresponds to Si/Al ratios of >3, while "Al-rich" corresponds to Si/Al ratios of <3 but >1.5, which is a criterion for X and Y zeolites.[21,22,44] For ZSM-5 (**MFI**) zeolite, "high-silica "usually refers to Si/Al ratios of >20 and the "Al-rich" usually refers to Si/Al ratios of <15.[45,46] Thus, the difficulty in tuning the Si/Al ratios depends on zeotype structures. For example, the range of the Si/Al ratios for Y zeolite is narrow, while that for ZSM-5 is broad. Generally, the Si/Al ratios of a zeolite cannot be lower than 1 because of the limitation of the Löwenstein rule.[43,47,48]

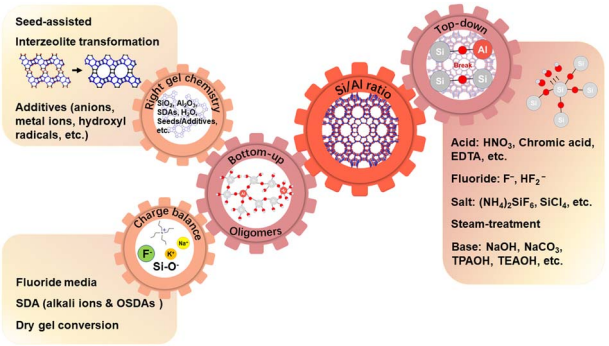

Fig. 1 Principles and methodologies for regulating the Si/Al ratios of zeolites.

2.1. "Bottom-up" tuning of the Si/Al ratios of zeolites

The "bottom-up" strategy for tuning the Si/Al ratios of zeolites is mostly performed by changing the Si/Al ratios of the synthetic mixture. The Si/Al ratios of the oligomers can be modified by various methods which can be divided into two categories. One category is associated with altering the gel chemistry such as by altering the gel composition *via* modifying the recipe or dissolving the parent zeolites and introducing additives to promote the formation of Si–O or Al–O bonds.[42,49,50] The other category is associated with the principle of charge balance. As mentioned above, the negative charges of the framework of zeolites originated from the substitution of Si^{4+} by Al^{3+}, which have to be balanced by the positive charges. Hence, the number of Al atoms equals the number of compensated positive charges provided by inorganic and/or organic extra-framework cations. In the end, fluoride, organic structure-directing agents (OSDAs) and dry gel conversion (DGC) can alter the Si/Al ratios of zeolites by following the principle of charge balance in which defects with negative charges can be easily formed in the DGC process.

As mentioned above, directly changing the Si/Al ratios of the synthetic mixture can accordingly alter the Si/Al ratios of the oligomers, resulting in the corresponding modification of the Si/Al ratios of a zeolite framework. For example, ZSM-5 (**MFI**-type) with Si/Al ratios ranging from 20 to 220 can be obtained by directly tuning the Si/Al ratios of the synthetic mixture in the presence of the OSDA tetrapropylammonium ions (TPA^+).[51,52] However, an unusually high concentration of Al or Si in the

synthetic mixture can slow down the crystallization process, which often requires a longer time to complete the crystallization.[53–55] For example, ***BEA**-type zeolites with Si/Al ratios from 25 to ∞ can be synthesized from a synthetic mixture with the molar composition of $0.35Na_2O : 4.5(TEA)_2O : xAl_2O_3 : 25SiO_2 : 295H_2O$, using a tetraethylammonium cation (TEA^+) as the template, where x is varied between 0 and 0.50.[54] The complete crystallization of the high-silica Beta zeolite needs a longer time compared to the Al-rich Beta zeolite. For example, three days are needed for the crystallization of Beta zeolite with Si/Al ratios of 25, 50, and 83 and five days are needed for the Beta zeolite with a Si/Al ratio of 250, while 11 days are needed for the pure silica Beta zeolite.

However, if the gel chemistry of the synthetic mixture deviates too far from the optimal one due to the modification of the Si/Al ratios of the synthetic mixture, the target zeolites will usually not be formed no matter how long the crystallization time is prolonged. In such cases, introducing the seed, which can promote the nucleation of the synthetic mixture, usually helps the formation of the target zeolites with desired Si/Al ratios.[56–58] For example, if the Si/Al ratios of a synthetic mixture for the crystallization of ***BEA** zeolite are significantly decreased from their optimal value in order to synthesize Al-rich Beta, the competitive **MOR** zeolite becomes the main product, while introducing Beta seeds to the same synthetic mixture resulted in the crystallization of Al-rich Beta with Si/Al ratios of 4–6.[42,55,59] By utilization of K-**CHA** seeds, phase pure Al-rich **CHA** (Si/Al = 1.6–2.0) can be synthesized from an Al-rich synthetic mixture, which produces **CHA** zeolite and an impurity in the absence of K-**CHA** seeds.[58] Liu and co-workers reported for the first time the synthesis of high-silica ZSM-35 (Si/Al = 14.5) with high solid yield (65–85%) by using the as-synthesized MCM-49 (Si/Al = 9.55) as seeds, while an amorphous product and **MOR** zeolite were obtained in the absence of MCM-49 seeds after crystallization of the same initial reaction mixture for 16 and 40 h, respectively.[60] The high-silica zeolite Y with a Si/Al ratio of up to 7.95 can be synthesized with the seed-assisted strategy, while only an amorphous product was obtained in the absence of seeds.[61] Xiao and co-workers also successfully synthesized pure silica zeolites (**MFI**, **MTT**, **TON**, and ***MRE**) and ZSM-5 zeolites with Si/Al ratios ranging from 38 to 240 by using such a strategy (besides zeolite seeds, alcohol as the space filler was also used).[62,63] Therefore, the successful assembly of oligomers with appropriate Si/Al ratios is the key to forming zeolites with desired Si/Al ratios.

Interzeolite transformation has been proven to be an efficient strategy for zeolite synthesis.[64] Such a strategy can also be used to tune the Si/Al ratios of target zeolites because the released locally ordered aluminosilicate oligomers from parent zeolites might facilitate the formation of another zeolite with unusual Si/Al ratios under appropriate conditions.[65] For example, high-silica **OFF** zeolites can be synthesized *via* interzeolite transformation in an aqueous solution containing benzyltrimethylammonium hydroxide (BTMAOH) and alkali metal hydroxide at 125 °C by solely tuning the Si/Al ratios of the parent **FAU** zeolites without introducing additional Si and Al sources (*i.e.*, Si/Al = 23 (**FAU**) → 7.6 (**OFF**); 31 (**FAU**) → 8.0 (**OFF**)).[66] Interestingly, high-silica **CHA** can be obtained after crystallization for 7–21 days (*i.e.*, Si/Al = 16 (**FAU**) → 14.5 (**CHA**); 22 (**FAU**) → 18.2 (**CHA**); 30 (**FAU**) → 21.5 (**CHA**)) if the **CHA** seeds were introduced into the same synthesis system.[67] Moreover, high-silica **CHA** (Si/Al = 10.5–11.4) zeolites can be transformed from **FAU** (Si/Al = 10.8) zeolite under a solvent-free system within 24 h in the presence of the OSDA *N*,*N*,*N*-dimethylethylcyclohexylammonium bromide (DMCHABr), **CHA** seeds, and NaOH.[68] However, only amorphous products were obtained under identical conditions if the parent **FAU** zeolites were replaced by equivalent chemicals which demonstrated that the appropriate distribution of the oligomers with specific Si/Al ratios and specific structures in the synthetic mixture is critical for the formation of **OFF** or **CHA** zeolites with target Si/Al ratios.

In interzeolite transformation, sometimes additional Si and Al sources and seeds are needed to achieve a successful interzeolite transformation. For example, Li and co-workers synthesized high-silica **CHA** zeolite with higher Si/Al ratios (*i.e.*, Si/Al > 30) *via* interzeolite transformation in the presence of the OSDA *N*,*N*,*N*-trimethyladamantammonium hydroxide (TMAdaOH), the seed of zeolite L with a Si/Al ratio of 3, and additional Si and Al sources, making a Si/Al ratio of 42.85 in the initial mixture.[69] Besides high-silica **CHA**, Al-rich **CHA** (Si/Al = 1.5–1.7) zeolites can also be synthesized *via* interzeolite transformation from the **FAU** (Si/Al = 2.6) zeolite along with an additional $Al(OH)_3$ source.[70] In the synthesis of high-silica Beta zeolite *via* **FAU** interzeolite transformation, it was found that the transformation was not successful if the Si/Al ratios of **FAU** were higher than 69.[71] Considering that the **MOR** zeolite and Beta zeolite have similar building units, Wu and co-workers prepared the high-silica Beta zeolite with a Si/Al ratio of 146, 216, 254, 296, and 357 *via* interzeolite transformation of the high-silica **MOR** zeolite with a Si/Al ratio of 145, 213, 255, 298, and 353, respectively, in the presence of tetraethylammonium hydroxide (TEAOH) and fluoride ions (Fig. 2).[49] These results clearly demonstrate that the right gel chemistry combined with the seeding strategy if necessary is of the utmost importance to regulate the Si/Al ratios of the resultant zeolites, which can be achieved *via* modifying the recipe of the initial reaction mixture or interzeolite transformation.

Besides changing the Si/Al ratios of the initial mixture or dissolving the zeolites to modify the Si/Al ratios of the

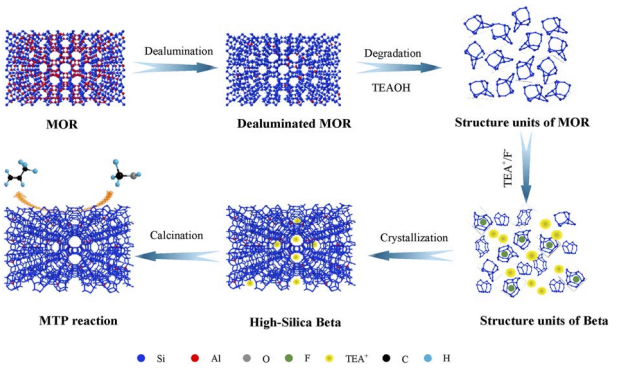

Fig. 2 Synthesis of high-silica Beta zeolite *via* interzeolite transformation of high-silica MOR zeolite. Reproduced from ref. 49 with permission from Elsevier, Copyright 2021.

oligomers, introducing extra species to alter the condensation of Si–O–Si(Al) bonds, such as anions, metal ions, and hydroxyl radicals can also modify the Si/Al ratios of the oligomers and further regulate (mostly increase) the Si/Al ratios of the resultant zeolites. Guided by this principle, Yu and co-workers reported a general and facile strategy to improve the Si/Al ratios of **MOR**, **FAU**, and **MFI** zeolites by adding iodide ions into the initial mixture, which promoted the formation of Si–O–Si bonds and thus provided a high-silica oligomer.[72,73] Shen and co-workers introduced Co^{2+} into the initial mixture for the OSDA-free crystallization of zeolite Y.[44] The introduced Co^{2+} forms a 5-coordinated intermediate (Co–O–Si)* with the silicate species. Such intermediate interferes the formation of the Al–O–Si species but has less influence on the formation of Si–O–Si species, resulting in the high Si/Al ratios of aluminosilicate oligomers in the initial mixture and the increased SiO_2/Al_2O_3 ratio of the produced zeolite Y to 6.15. Yu and co-workers discovered that hydroxyl radicals (˙OH) can facilitate the dissociation of the Si–O–Si bonds and promote the remaking of Si–O–Si bonds.[74] In terms of such an effect of ˙OH, Yu and co-workers introduced ˙OHs *via* hydrogen peroxide into the initial mixture for the OSDA-free crystallization of zeolite Y with a SiO_2/Al_2O_3 ratio of 6.35, overcoming the upper limit of 6.0 for synthetic zeolite Y by a one-step organic-free route.[50] The condensation of $Si(OH)_3ONa$ and $Al(OH)_4Na$ monomers with $Si(OH)_3O^{\cdot}$ and $Si(OH)_2ONaO^{\cdot}$ radical species was studied using density-functional theory (DFT) calculations (Fig. 3). The calculated Gibbs free energies (Fig. 3c) indicated that the $Si(OH)_3O^{\cdot}$ radical preferentially accelerated the formation of Si–O–Si bonds. Furthermore, nanosized Beta zeolites with Si/Al ratios ranging from 6 to 300 were obtained by a facile L-lysine assisted method.[75] In such a synthetic system, L-lysine can chelate the silica and aluminum precursors. Attachment of L-lysine to the oligomers inhibits the growth of zeolites and prevents the formation of impurities. These results demonstrate that the additionally introduced species possessing the ability to modify the Si/Al ratios of the oligomers can also regulate the Si/Al ratios of the resultant zeolites.

The synthesis of zeolites usually involves a silicon source, an aluminum source, alkali hydroxide, and water. OH^- from alkali hydroxide acts as a mineralizer that promotes the formation of Si–O–Si and Si–O–Al bonds resulting in negatively charged aluminosilicate oligomers, which are assembled around alkali cations to form long-range ordering structures of zeolites. As mentioned above, the number of compensated alkali cations equals the number of Al atoms in the framework of zeolites, and the zeolites directed by the alkali hydroxide are mostly Al-rich due to the high charge density of alkali cations.[23,76] Therefore, replacing the high charge density cation with low charge density organic quaternaryammonium and/or the mineralizer OH^- with another mineralizer F^- in the form of hydrogen fluoride (HF) can decrease the incorporation of Al into the framework of zeolites, which can thus increase the Si/Al ratios of the resultant zeolites.[77,78] Taking this principle into consideration, Liu and co-workers synthesized high-silica Beta zeolites with various Si/Al ratios (Si/Al = 130 to 340) in the presence of fluoride ions and TEAOH.[79] Moreover, pure silica Beta zeolite can be obtained from a fluoride medium with TEAOH as OSDA under extremely low water content conditions.[80]

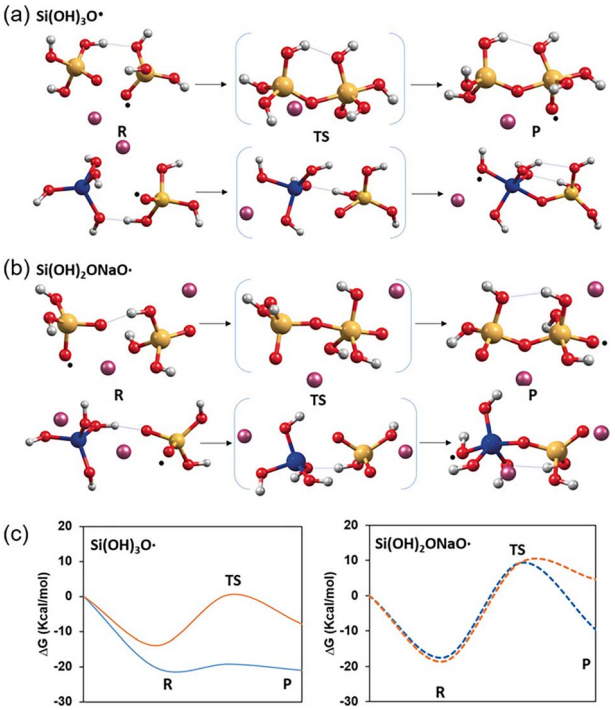

Fig. 3 Optimized geometries of the structures involved in the condensation of (a) $Si(OH)_3O^{\cdot}$ and (b) $Si(OH)_2ONaO^{\cdot}$ radical species with $Si(OH)_3ONa$ and $Al(OH)_4Na$. Si, Al, O, H, and Na atoms are depicted as yellow, blue, red, white and purple spheres, respectively. (c) Corresponding Gibbs free energy profiles for condensation of radicals with $Si(OH)_3ONa$ (blue) and $Al(OH)_4Na$ (orange). Reproduced from ref. 50 with permission from Wiley, Copyright 2020.

Zeolites directed by OSDAs usually have higher Si/Al ratios than those directed by inorganic cations such as Na^+ and K^+ because the charge density of an OSDA is usually lower than that of inorganic cations. Compared to OSDA cations, more inorganic cations can be accommodated in the same pore or cavity of the zeolite, which needs more Al atoms to be incorporated into the oligomers, finally resulting in lower Si/Al ratios.[23] Unlike inorganic cations possessing similar charge densities, organic cations' charge densities vary widely. Thus, the Si/Al ratios of zeolites can be tuned by varying the charge density of organic cations. Basically, the upper limit of the Si/Al ratio for Y zeolite synthesized by a one-step organic-free route is 3, which was broken by Yu and co-workers *via* introducing ˙OHs into the synthetic system.[50] However, there are kinetic limitations for the synthesis of Y zeolite with high Si/Al ratios because the crystallization rate decreases with increasing Si/Al ratios of the Y zeolite.[81] Y zeolite with a Si/Al ratio approaching 5 was synthesized by using crown-ether based supramolecules as OSDAs in 1990.[82] Subsequently, high-silica Y zeolite with various Si/Al ratios had been reported by using *N*-methylpyridinium (NMP) iodide (Si/Al = 3.18–3.43),[83] imidazolium-based ionic liquid (Si/Al = 3.2–3.4),[84] TEAOH (Si/Al = 3.88),[85] and choline (Ch, Si/Al = 3–6).[30,86] Recently, Liu and co-workers reported that increasing the TBA^+/TEA^+ (TBA^+: tetrabutylammonium cations) ratio from 1.3 to

4.0 results in an increase in the Si/Al ratio of Y zeolite from 5.1 to 7.8.[23] Using the bulky organic cation of 4,4′-trimethylenebis(*N*-methyl, *N*-benzyl-piperidinium) (TMP) as the OSDA, purely siliceous ***BEA** can be synthesized in alkaline media with a molar composition of 1 SiO_2 : x $TMP(OH)_2$: 25 H_2O (x = 0.15–0.30) at 90–100 °C.[87] Similarly, Corma and co-workers synthesized nanosized high-silica Beta zeolites with solid yields of over 95% by using alkyl-substituted flexible dicationic OSDAs such as 1,1′-(pentane-1,5-diyl)bis(1-butylpyrrolidin-1-ium) and 1,1′-(pentane-1,5-diyl)bis(1-butylazepan-1-ium).[88]

Besides high-silica zeolites, combining OSDAs and fluoride can result in the formation of pure-silica zeolites. Zeolite A (**LTA**) crystallized from an OSDA-free synthesis system is highly Al-rich and the typical Si/Al ratio is one.[89] Using tetramethylammonium (TMA^+) and tetraethylammonium (TEA^+) as structure-directing agents (SDAs) instead of alkali cations increased the Si/Al ratio of zeolite A to 3.2.[90] Notably, pure-silica **LTA** (ITQ-29) zeolite can be obtained in the presence of fluoride and the combined OSDAs of methylated julolidine and TMA.[91] Subsequently, high/pure-silica **LTA** zeolites were synthesized from an initial mixture containing fluoride and TMA/imidazolium-based OSDAs.[92–94] In addition, Hong and co-workers successfully synthesized high-silica **UFI** zeolite (Si/Al = 11) and **LTA** zeolites (Si/Al = 8.3 to ∞) in fluoride media together with benzylimidazolium-based OSDAs.[94]

Besides hydrothermal synthesis, dry gel conversion (DGC) is another main method to synthesize zeolites, which was first reported by Xu and co-workers in 1990.[95] Unlike the hydrothermal synthesis containing a large amount of water, the DGC method contains only a very limited amount of water, which may moderate the species transportation and thus leave abundant defects (*e.g.*, $Si–O^-$) with negative charges, which can balance the positive charge of the OSDA. Thus, high-silica and even pure-silica zeolites can usually be obtained by the DGC method even in the absence of fluoride.[96] For example, the Si/Al ratios of SSZ-13 (**CHA**) typically range from 10 to 54. However, Miyake and co-workers increased the Si/Al ratios of SSZ-13 up to 182 by the DGC method.[97] Recently, Fan and co-workers reported that the charge-balancing interactions between an inorganic cation, OSDA, and $Si–O^-$ defects by the DGC method are essential aspects for the synthesis of fluoride-free siliceous **CHA**, **STT**, ***BEA**, **MFI**, and ***MRE**.[98] Very recently, pure-silica Beta was also fabricated by DGC with a dry gel composition of SiO_2 : 0.16NaOH : 0.08TEAOH.[99]

Table 1 summarizes the representative examples of regulating the Si/Al ratio and their influence on the performance with "bottom-up" methods. "Bottom-up" methods provide a one-pot methodology to regulate the Si/Al ratios of zeolites which avoids destroying the framework but is not easily amenable to industrialization since they involve substantial amounts of costly templates, emissions of waste liquor, and complicated operating steps.[32]

2.2. "Top-down" tuning of the Si/Al ratios of zeolites

Regulating the Si/Al ratios of zeolites means tuning the Si/Al ratios of the zeolite crystals (*i.e.*, the final products). "Top-down" means tuning the Si/Al ratios on the basis of already synthesized zeolite crystals, which is mostly realized by post-treatment methodologies. In addition, for the aluminosilicate framework of zeolites, the Al or Si within the framework can be selectively removed to modify the Si/Al ratios of a zeolite, which is also termed "post-synthesis" or "post-treatment". Compared to the "bottom-up" strategy, the "top-down" strategy has the advantages of facile operation and easy scale-up, but it will inevitably cause a significant decrease in the crystallinity of zeolites, resulting in plenty of defects and silanol groups.

The foundation of the "top-down" strategy is that the tension of the tetrahedral sites (T-sites) in the framework of a zeolite is not uniform throughout the framework and depends on its position, which makes it possible to selectively remove Si (desilication) or Al (dealumination).[100–103]

The routes for the dealumination of zeolites *via* post-modification include acid, fluoride, steam, and salt treatment. During dealumination by acid treatment, Al species with high tension are dissolved using an acid. However, the framework of the zeolite may collapse in nitric acid if the Si/Al ratio is too low. The successful dealumination in nitric acid has been applied to ***BEA**, **FAU**, and **MOR**.[104–109] In the dealumination of Beta zeolites, the Si/Al ratio was increased to over 200 if the starting Si/Al ratio was greater than 12, while the framework collapsed if the starting Si/Al ratio was less than 12.[105] Besides nitric acid, many other acids and chelates can also be used in the dealumination of zeolites, such as oxalic acid,[109–112] ethylene diamine tetraacetic acid (EDTA),[103,107,113] and hydrochloric acid.[103,107] For example, Valtchev and co-workers recently reported the mild dealumination of zeolites with chromic acid.[114] The Si/Al ratio of 9.0 of the parent **CHA** zeolite was increased to 9.4 and further to 10.5, while the Si/Al ratio of the **MFI** zeolite was increased to 21 from 19. During mild dealumination, the framework was well preserved and Brönsted acid sites (BASs) were preserved and their accessibility was increased. Moreover, Fan[103,115,116] and Yu[117] developed a microwave-assisted dealumination method which can significantly reduce the treatment time from at least 6 h *via* conventional hydrothermal treatment to several minutes and generate mesoporous structures. However, sequential alkaline desilication was needed after the dealumination treatments to recover the zeolitic framework and generate mesopores in the treated zeolites.

As mentioned above, fluoride has been widely used in the synthesis of high- or pure-silica zeolites.[77–80,93,94] Considering the strong affinity of fluorine with Si and Al, fluoride can also be used in tuning the Si/Al ratios of zeolites *via* desilication or dealumination. However, the pH of the solution needs to be carefully controlled to prevent framework collapse when hydrogen fluoride (HF) is used. Besides HF, NH_4F,[102,118,119] NaF,[119,120] $NaHF_2$,[119,121] and NH_4HF_2 [102,119] have also been used as the sources of fluoride. Moreover, dealumination by F^- or HF_2^- can also generate secondary porosity.[102,119,120,122] $(NH_4)_2SiF_6$ is also a widely used dealumination agent,[123] which can not only extract aluminium from the framework but also serve as an extraneous source of silicon that can fill up the vacancies created in the framework by the extraction of aluminium.[123–127] For example, Yokoi and co-workers tuned the Si/Al ratio of Al-rich Beta to 73 and removed more than 40% of the Al atoms of

Table 1 Summary of the representative examples of regulating the Si/Al ratio and their influence on the performance with "bottom-up" methods

Topology	Methods	Si/Al (SiO_2/Al_2O_3)[a]	Influence on performance	Ref.
FAU (Y)	Regulating the recipe	1.5–3	—	21, 22 and 44
	Seed-assisted strategy with smaller seed size and higher seed Si/Al ratios	7.95 (15.9)	Higher conversion in heavy oil cracking than ultra-stable Y	61
	I^- facilitating the formation of Si–O–Si bonds	2.66 (5.32)	N/A	72
	Increasing the Si/Al ratio of the fragments around the additionally introduced Co^{2+}	3.08 (6.15)	The catalytic cracking performance of this sample is significantly higher than that of the ordinary NaY	44
	Hydroxyl radicals ($^•OH$) facilitating the formation of Si–O–Si	3.18 (6.35)	N/A	50
	OSDA (crown-ether based supramolecules)	Approaching 5	N/A	82
	High crystallization temperature (130 °C) and *N*-methylpyridinium as the OSDA	3.18–3.43 (6.35–6.85)	N/A	83
	OSDA (TEA^+)	3.88 (7.76)	N/A	85
	OSDA (Ch^+)	3–6	N/A	30 and 86
	OSDA (TBA^+ and TEA^+)	5.1–7.8(10.2–15.6)	Higher conversion and C4 selectivity in catalytic cracking of hydrocarbons	23
***BEA** (Beta)	Regulating the recipe	4–6	N/A	39–41
	OSDA (TEA^+)	25 to ∞	N/A	54
	OSDA-free with the aid of beta seeds	4–6	N/A	42, 55 and 59
	MOR interzeolite transformation in fluoride media using an OSDA (TEA^+)	146–357	Long lifetime and high propylene selectivity in the methanol to propylene (MTP) reaction	49
	HF assisted method and OSDA (TEA^+)	130–340	Suppressing the formation of aromatics in the MTP reaction The longest catalytic lifespan in the MTP reaction	79
	OSDA (TMP)	∞	N/A	87
	Dry-gel-conversion method with a small amount of OSDA (TEA^+)	∞	N/A	99
CHA (SSZ-13)	Regulating the recipe	10–54	N/A	97
	KCHA seeds	1.6–2.0	N/A	58
	FAU interzeolite transformation with **CHA** seeds	14.5–21.5	A maximum propylene yield (48%) was achieved at a Si/Al ratio of 15 in the ethanol to olefins (ETO) reaction	67
	FAU interzeolite transformation with an OSDA (DMCHABr) and **CHA** seeds	10.5–11.4	The Cu^{2+} ion-exchanged catalyst shows nearly 100% conversion of NO in the temperature range of 200–350 °C	68
	OSDA (TMAdaOH), zeolite L (Si/Al = 3) interzeolite transformation, and additional Si and Al sources	>30	Good catalytic performance in the methanol to olefins (MTO) reaction	69
	FAU interzeolite transformation and an additional $Al(OH)_3$ source	1.5–1.7	N/A	70
	Dry-gel-conversion method (DGC)	182	N/A	97
MOR	I^- facilitating the formation of Si–O–Si bonds	7.08 (14.15)	N/A	72
LTA	Regulating the recipe	1	N/A	89
	OSDAs (TEA^+ and TMA^+)	3.2	N/A	90
	OSDAs (methylated julolidine and TMA^+) and fluoride media	∞	N/A	91
	OSDAs (TMA and imidazolium-based OSDAs) and fluoride media	16 to ∞	The Cu^{2+} ion-exchanged high-silica (Si/Al ∼ 17) **LTA** hydrothermally aged at 900 °C showed better activity maintenance for selective catalytic reduction of nitrogen oxides with ammonia (NH_3-SCR) than Cu-SSZ-13	92–94

[a] SiO_2/Al_2O_3 used in the original research is listed in parentheses.

MCM-22 by treating it with $(NH_4)_2SiF_6$ solution.[126,128] Furthermore, $(NH_4)_2SiF_6$ has also been used to increase the Si/Al ratios of **MOR**, **FER**, Y, ZSM-5, and SSZ-13 zeolites *via* dealumination with simultaneous silicon reinsertion.[124,125,127,129]

Similar to $(NH_4)_2SiF_6$, $SiCl_4$ vapour has the ability to extract the Al atoms from the framework of zeolites and simultaneously insert the Si atoms derived from $SiCl_4$ into the vacancy due to the removal of Al, which results in an increase in Si/Al ratios.[130] In the 1980s, Beyer and co-workers first developed such a method.[131–133] With this method, highly siliceous Y zeolites (Si/Al = 3.3–63) were obtained.[131,134,135] However, this method is not commonly used because of the harsh operating conditions.

In solution, $Al_2(SO_4)_3$ can react with the framework Al of zeolites containing Na^+ to form the mineral natroalunite ($NaAl_3(SO_4)_2(OH)_6$), resulting in the extraction of the framework Al and thus an increase in Si/Al ratios.[136] With this method, the Si/Al ratio of the framework of NaY can be increased to 4.2 from 2.4, while that of Beta zeolite can be increased up to 12.4 from 4.6.[43,136]

Besides reacting with the framework Al of zeolite, breaking the Al–O bonds can also lead to the removal of the framework Al. In fact, water in steam form can break the Al–O bonds *via* hydrolysis (Fig. 4).[137] Based on this knowledge, steaming dealumination of zeolite has been developed, which has been commercialized for preparing ultra-stable Y zeolite (USY), a revolutionary fluid catalytic cracking (FCC) catalyst.[138] Besides Y zeolite, Hutchings and co-workers dealuminated the **MOR** zeolite *via* steaming and increased the Si/Al ratio of the **MOR** zeolite to 16.6 from 7.5.[139] At the same time, Morin and co-workers prepared a series of dealuminated **EMT** zeolites with Si/Al ratios of 5.5, 7.6, 13, 31, and 52 from the NH_4 type **EMT** with a Si/Al ratio of 4.5 by steaming for various times (0.5–3 h) at various temperatures (450–650 °C).[140] Recently, Yang and co-workers prepared dealuminated H-**MOR** (Si/Al = 15.26, 25.13, 40.65) and dealuminated Na-**MOR** (Si/Al = 9.96, 11.20, 12.61) by steaming H-**MOR** (Si/Al = 8.74) and Na-**MOR**, respectively, which increased the availability of acid sites in the side pockets of **MOR** zeolite.[141]

Dealumination of zeolites can increase their Si/Al ratios, while desilication can decrease their Si/Al ratios. It is well known that hydroxide ions (OH^-) can effectively break the Si–O–Si bonds. Thus, alkaline solution treatment of zeolites can remove the Si atoms from the framework, which certainly reduces the Si/Al ratios[142,143] and thus forms mesopores within the zeolite crystals.[45,144–152] To date, the inorganic bases NaOH[45,100,111,142,147–155] and Na_2CO_3 [145] have been used for the desilication of zeolites. For example, Bjørgen and co-workers produced ZSM-12 with Si/Al ratios of 13–34 by treating calcined ZSM-12 (Si/Al = 39) with 0.2–0.6 M NaOH solutions at temperatures of 35 °C, 65 °C, or 85 °C for durations of 15 to 60 min.[156] Besides inorganic bases, organic bases, such as TBAOH,[154,155] TEAOH,[149,151] and TPAOH, can also be used for the desilication of zeolites and generation of intracrystalline mesopores in zeolites.[146]

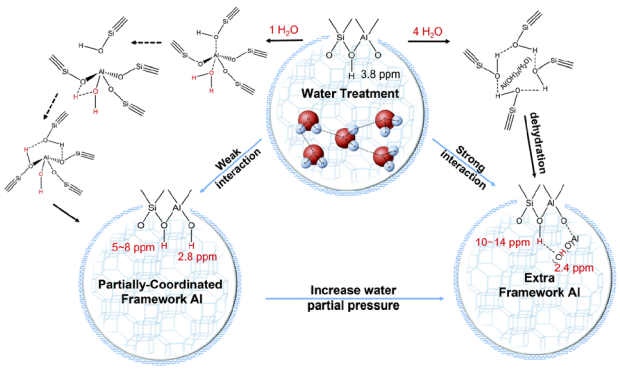

Fig. 4 Proposed mechanism of the dealumination process induced by hydrothermal-treatment of SSZ-13 zeolite. Reproduced from ref. 137 with permission from the Royal Society of Chemistry, Copyright 2022.

2.3. Methods for determining the Si/Al ratios of zeolites

The commonly used analytical techniques for determining the Si/Al ratios of zeolites include X-ray fluorescence spectroscopy (XRF), atomic absorption spectroscopy (AAS), inductively coupled plasma atomic emission spectroscopy (ICP-AES), X-ray diffraction (XRD), solid state ^{29}Si magic-angle-spinning nuclear magnetic resonance spectroscopy (^{29}Si MAS NMR), X-ray photoelectron spectroscopy (XPS), energy-dispersive X-ray spectroscopy (EDS), electron probe micro-analysis (EPMA), and newly developed Fourier-transform infrared spectroscopy (FT-IR).[157]

Generally, chemical analyses such as ICP-AES and AAS determine bulk Si/Al ratios. However, the XRD, FT-IR, and NMR analyses can also be used to determine the framework Si/Al ratios. XPS as well as EDS and EPMA are used to determine the surface or local Si/Al ratios which have poor sampling depths or rely on the electron penetration of a beam.[158,159]

XRF has been widely used to determine the Si/Al ratios of zeolites.[42,61,103] The features of XRF analysis are accuracy, rapidity, multielement capacity, and nondestructiveness.[160] However, XRF analysis is a surface-sensitive method, and the penetration depth of the primary radiation is about μm or so for low-Z elements and about 100 μm or so for heavy elements.

AAS is a routine but widely and frequently used tool in determining the metal and metalloid concentrations dissolved in solution. It offers sufficient sensitivity and is relatively interference free, which has been used to determine the Si/Al ratios of zeolites.[161–163] An ICP-AES is one of the most popular instruments in chemical laboratories, which can determine more than 70 elements with detection limits in the parts per billion (ppb) to parts per million (ppm) range and offers very high throughput and the capacity of multiple reportable results per run. Compared to AAS, ICP-AES is especially suitable for refractory elements, such as Si and Al, which are analysed poorly by flame AAS.[52,112,164] However, analysis of Si and Al by AAS and ICP-AES requires the complete dissolution of zeolite samples into solution, which usually involves toxic hydrofluoric acid. This is the disadvantage of AAS and ICP-AES.

Due to the non-negligible difference in the bond lengths between Si–O and Al–O bonds, for Y zeolite for example, the change in Si/Al ratios may lead to the change of the specific

crystal plane, which thus modifies the cell parameters and shifts the position of specific X-ray diffraction peaks. On the basis of this fact, X-ray diffraction analysis has been widely used as an important and convenient method to determine the Si/Al ratios of Y zeolites.[50] With this method, Hajjar and co-workers reported that the d_{302} spacing of ***BEA** zeolites decreased along with an increase in the Si/Al ratio from 3.955 Å (Si/Al = 11; 2θ = 22.55°) to 3.939 Å (Si/Al = 46; 2θ = 22.57°), 3.929 Å (Si/Al = 87; 2θ = 22.63°), 3.922 Å (Si/Al = 135; 2θ = 22.69°), and finally to 3.920 Å (Si/Al = 1240; 2θ = 22.71°).[165]

Solid state ^{29}Si MAS NMR spectroscopy plays an important role in probing various aspects of zeolite structures. In the framework of zeolites, Si is tetrahedrally coordinated. Considering all possibilities, there are five different environments for framework Si atoms depending on the number of adjacent O–Al atoms, which are denoted as Si(nAl) (n = 0, 1, 2, 3, 4). According to the ^{29}Si MAS NMR spectrum, the Si/AI ratios in the zeolite framework can be calculated as follows:

$$(\mathrm{Si/Al})_{\mathrm{NMR}} = \sum I_{\mathrm{Si}(n\mathrm{Al})} / \sum 0.25 n I_{\mathrm{Si}(n\mathrm{Al})} \quad (1)$$

where $I_{\mathrm{Si}(n\mathrm{Al})}$ is the intensity of the NMR signal attributable to the Si(nAl) units, and the summation is from n = 0 to n = 4.[166] The Si/Al ratios determined by solid state ^{29}Si MAS NMR are consistent with those measured by elemental analysis.[24,72,141] By comparing the $(\mathrm{Si/Al})_{\mathrm{NMR}}$ values with those obtained by chemical analyses, the amount of extra-framework aluminium can be calculated. However, eqn (1) works well with materials that have framework Si/AI ratios of less than about 10. It cannot be directly applied to the spectra in which signals coming from Si(nAl) units of crystallographically nonequivalent Si atoms overlap, such as the spectrum of omega zeolite.[166–168]

Determining the Si/Al ratios of zeolites by FT-IR is a recently developed technique.[157,169] In the FT-IR spectrum of zeolites, the vibrations associated with the framework structure are present in the mid IR region (200–1300 cm^{-1}). The T–O–T asymmetric stretching band associated with the framework is sensitive to the Al content. As shown in Fig. 5, the skeletal stretching vibrations shift to higher frequencies along with an increase in Si/Al ratios.[170,171] A recent study combined the chemometric methods of partial least squares (PLS), support vector machines (SVMs), and soft independent modelling of class analogy (SIMCA) to quantify the Si/Al ratio in zeolites based on FT-IR spectra.[169] Before this tentative finding, Fichtner-Schmittler and co-workers found a linear relationship for **FAU** zeolite between the unit cell parameter a_0 and the framework vibrations over the whole range of Si/Al ratios (Si/Al < 10) with an error of <10%:[172]

$$\frac{\mathrm{Al}}{\mathrm{Al}+\mathrm{Si}} = 0.59 a_0 \ \left(\text{Å}\right) - 14.3 = 4.68 - 4.30 \times 10^{-3}\ \bar{\nu}_{\mathrm{as}}\ \left(\mathrm{cm}^{-1}\right) \quad (2)$$

where $\bar{\nu}_{\mathrm{as}}$ is the wavenumber of an asymmetric stretching band. Later, Lohse and co-workers observed another linear relationship for Y zeolite between the Si/Al ratios and the vibrational band ν_3 at 748–837 cm^{-1}:

$$\mathrm{Al/(Al + Si)} = 0.029 - 4.30 \times 10^{-3} \Delta\nu_3\ (\mathrm{cm}^{-1}) \quad (3)$$

where $\Delta\nu_3$ is the difference between the wavenumbers ν_3 of the recorded sample and the standard Y zeolite (Si/Al = 2.4).[170] Recently, Ng and co-workers developed an IR-based protocol to determine the Si/Al ratios of 19 kinds of zeolites.[157] The authors proposed a linear equation of $y = 0.0458x - 43.584$, where y is the Si/Al ratio and x is the asymmetric stretching frequency of the Si–O–T band (cm^{-1}). The equation is valid for Si/Al ratios between 1 and 5. Very recently, Sadrara and co-workers combined the FT-IR spectra, partial least squares, and support vector machines to quantify the Si/Al ratios of zeolites ZSM-5, **MOR**, and ZSM-48 with high accuracy.[169]

XPS is an elemental analysis technique that is a surface-sensitive technique with a sampling depth of only a few nanometres.[159] With this technique, Rimer and co-workers determined the shell thickness of core–shell **MEL** zeolites with ZSM-11 cores and passivated silicalite-2 shells (denoted as ZSM-11@silicalite-2) as shown in Fig. 6.[173] The Si/Al ratio of the shell is much higher than that of the core. The depth with a sudden drop in the Si/Al ratio was treated as the thickness of the shell. Scanning electron microscopy with energy dispersive X-ray spectrometry (SEM/EDS) is an elemental microanalysis technique widely applied in the determination of Si/Al ratios of zeolites.[174–176] However, high-reliability quantitative X-ray microanalysis by SEM-EDS needs a slim thickness (<50 nm) and standards.[158]

EPMA is well known as an analytic method that can acquire high quality and reproducible compositional data on individual zeolite grains. But sample heating and element mobility caused by the interactions between the electron beam and the sample result in dehydration and underestimation of light extra-framework cations as well as problems in determining the framework Si and Al, leading to subsequent inaccurate calculations of Si/Al ratios.[177,178]

2.4. Impact of Si/Al ratios on the performance of zeolites

The isomorphous substitution of a Si^{4+} by an Al^{3+} introduces a negative charge (polarity) to the framework of zeolites and a Brönsted acid site is obtained if this negative charge is balanced by a proton. The strength of Brönsted acid sites is

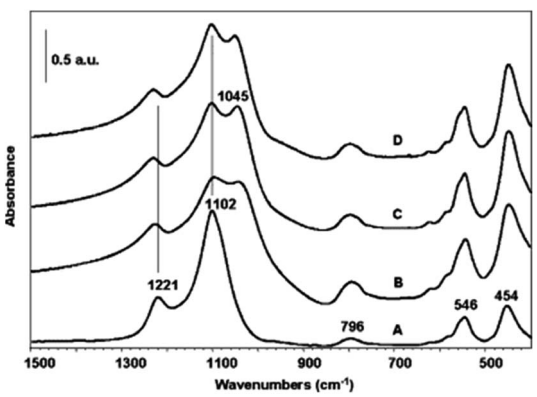

Fig. 5 FT-IR skeletal spectra of the ZSM-5 samples having different molar ratios of Si/Al (A, 18.5; B, 23.8; C, 43.0; D, 68.3). Reproduced from ref. 171 with permission from Elsevier, Copyright 2006.

stronger if they are more isolated from each other.[179] Thus, the content of Al^{3+} in the framework directly determines the amount (*i.e.*, concentration) and the strength of Brönsted acid sites. Moreover, the Si/Al ratios of zeolites can also affect the hydrophilicity/hydrophobicity, stability, and performance of zeolites on catalysis, adsorption, and ion-exchange.[18,23,164]

2.4.1. Catalysis. Fluid catalytic cracking (FCC) is one of the most important catalytic processes, which converts heavy petroleum to gasoline, diesel, and light gases. USY zeolite is the most efficient and important catalyst in FCC. In the catalytic cracking process, the catalyst needs to be circulated continuously between the reactor and the regenerator at high temperatures in the presence of steam, which requires the ultrastability of Y zeolite and thus higher Si/Al ratios of Y zeolite. To maximize the activity and selectivity, the Si/Al ratios of Y zeolites need to be optimized.[100,180] Therefore, the precise control of Si/Al ratios of Y zeolite has been attracting the researcher's interest. Recently, a series of high-silica Y zeolites have been prepared in the laboratory for cracking and pyrolysis.[24,61,100] Y zeolite with a Si/Al ratio of 8.0 exhibited higher conversion than two USY zeolites with Si/Al ratios of 5.3 and 6.9 in *n*-octane and 1,3,5-triisopropylbenzene (TIPB) cracking.[24] Compared to the USY zeolite with lower Si/Al ratios, the USY zeolite with higher Si/Al ratios has fewer acid sites. However, the remaining acid sites are strengthened, which increases the activity and the selectivity of cracking. Very recently, Liu and co-workers investigated the catalytic activity of HS-$SY_{14.3}$ (Y zeolite with a Si/Al ratio of 7.15) for TIPB cracking and cumene cracking.[61] Their results indicated that HS-$SY_{14.3}$ exhibited both high activity and high selectivity compared to the conventional Y zeolite because of the larger amount of acid sites and higher acid strength in HS-$SY_{14.3}$. The same group reported that the Y zeolite with Si/Al ratios of up to 8.0 possessed more strong acid sites than commercial USY with Si/Al ratios of 5.3 and 6.9. The former Y zeolite exhibited higher conversion and cracking depth in TIPB cracking and several times higher conversion in *n*-dodecane cracking than the latter USY reference.[23] In the co-pyrolysis of oil sludge and high density polyethylene (HDPE) catalysed by USY zeolites, Calderari and co-workers found that the catalytic cracking process followed a carbenium ion reaction mechanism, which was generated by the removal of a negative hydrogen ion from alkanes or the protonation of olefins.[100,181] The species containing carbenium ions cracked to small hydrocarbons on the BASs and Lewis acid sites of USY zeolites and resulted in the formation of new carbonium ions.[182,183] Recently, Shen and co-workers discovered that the dealuminated Beta zeolite generated more carbonium ions in the cracking of *n*-octane due to the enhanced strength of BASs, which is beneficial for hydrocarbon conversion.[184] Thus, enhancing the strength of the Brönsted acid by dealumination of zeolites *via* steaming can improve their catalytic properties for hydrocarbon activation.

Besides enhancing the strength of the Brönsted acid, dealumination of zeolite *via* steaming can also generate new species that can promote their catalytic performance. For example, Khivantsev and co-workers very recently observed the small alumina clusters of Al_1O_5 in the micropores of steam dealuminated **MFI** zeolite, which facilitated the C–H bond breaking of alkane and thus promote the cracking of C–C bonds over BASs.[185] Unlike the dealumination process that decreases the amount of BASs but enhances the strength of the remaining BASs, the desilication process generates more Lewis acid sites and mesopores thus increasing the total amount of acid sites and the accessibility of BASs but decreasing the strength of BASs.[154] As expected, the dedicated Beta zeolite with low acid strength had low activity on low-density polyethylene (LDPE) and *n*-octane cracking.[154,186]

Isomerization, oligomerization, aromatization, and alkylation of the hydrocarbons catalysed by the BASs of zeolites also follow the classical carbenium ion mechanism.[107,181] The performances of zeolite catalysts for these reactions strongly depend on the concentration and strength of BASs.[107,187–189] The quantity/concentration of BASs determine the number of active sites and the strength of the BASs governs the type of reaction. For example, the dealuminated Beta zeolite can catalyse isobutyl alcohol oligomerization and the conversion of isobutyl alcohol increases with an increase in the Si/Al ratios of Beta zeolite, which is controlled by the dealumination time.[107] However, the conversion of isobutyl alcohol decreases significantly if the Beta zeolite is treated by NaOH solution due to the significant loss of BASs. In the transformation of 2-butene, weak Lewis acid sites can result in double-bond migration, while the strong BASs can catalyse *cis–trans* and skeletal isomerization as well as oligomerization.[108] The former reaction is affected by the quantity of the BASs, while the latter reaction is affected by the strength of the BASs. As a result, the chain growth capacities of

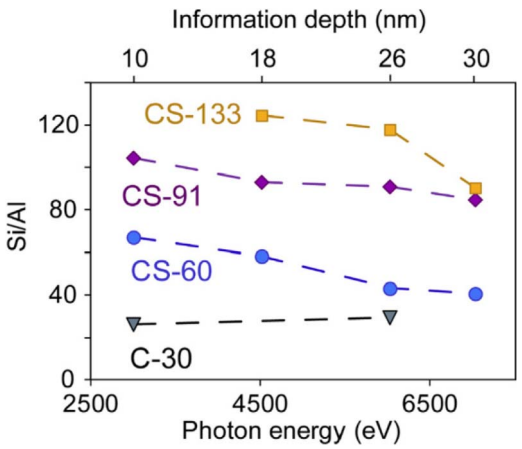

Fig. 6 Comparison of Si/Al ratios for a ZSM-11 core (C-30 with Si/Al = 30) and core–shell samples (CS-60, CS-91, and CS-133, and the corresponding Si/Al ratios of the shell are 60, 91, and 133) from XPS depth analysis (VKE-XPS) as a function of photon energy (bottom *x*-axis) and the corresponding information depth (top *x*-axis) where 95% of the signal is generated. Each sample was pre-coated with *ca.* 10 nm of carbon. Any uneven (or rough) surfaces of zeolite powders from VKE-XPS sample preparation increase the uncertainty in depth estimation for a single particle. This results in a diffuse transition between the shell and core that creates uncertainty in estimates of shell thickness. Reproduced from ref. 173 with permission from Elsevier, Copyright 2022.

the butene isomers in the oligomerization reaction catalysed by the untreated Beta zeolite are much higher than those catalysed by the dealuminated Beta zeolite.

Alkylation is catalysed by BASs and the distribution of products is affected by the strength of BASs. For example, lanthanum modified USY zeolite (La**FAU**) with a high Si/Al (Si/Al = 6.7) ratio possesses enhanced acid strength, which results in higher cracking and self-alkylation activity. Compared to the La**FAU** catalyst with a low Si/Al (Si/Al = 1.2) ratio, such high-silica La**FAU** yielded a lower C_8 production in isobutane alkylation.[190] Naphthalene *tert*-butylation with tertiary butanol can be catalysed by various dealuminated and/or desilicated **MOR** zeolites. However, first alkaline-treated and then acid-treated zeolites exhibited enhanced activities because the alkaline-treatment increased the accessibility of the active sites and the acid-treatment reduced the concentration of the strong BASs and increased the strength of the remaining BASs.[142] Palkovits and co-workers investigated the synthesis of oxymethylene dimethyl ethers (OME*x* oligomers with a chain length of *x*) over the zeolites ***BEA**, **FAU**, **MFI**, and **MOR** with various Si/Al ratios and observed a high turnover frequency for the zeolites with high Si/Al ratios.[191] As mentioned above, the Si/Al ratio of a zeolite not only determines the concentration/density but also the strength of the BASs. Thus, the optimal Si/Al ratio of a zeolite should be closely related to the specific reaction it catalysed. For example, Li and co-workers reported that ZSM-5 zeolites with lower Si/Al ratios have higher activity in the direct hydration of aromatic alkynes to ketones.[192]

Dimethyl ether (DME) is a reliable alternative fuel for compression ignition engines and can also be used as an intermediate to produce olefins and chemicals, which can be produced from the dehydration of methanol catalysed by the BASs of zeolites.[193–195] However, the trade-off effect between the activity and the selectivity is observed in such a reaction, depending on the Si/Al ratios of the zeolite catalyst.[196,197]

Hydrogenation of methyl acetate (MeOAc) that is formed *via* DME carbonylation is a new, efficient route to produce ethanol from syngas.[198] DME carbonylation can be catalysed by **MOR** zeolite in which BASs play an important role.[199,200] Yang and co-workers observed that dealuminated **MOR** zeolites exhibited low catalytic activity but high MeOAc selectivity, indicating that the low BAS density of mordenite is beneficial for the formation of MeOAc.[141] However, a trade-off effect was also observed in the DME carbonylation catalysed by the **MOR** zeolite, *i.e.*, the conversion of DME increased before the Si/Al ratio reached 11.8 and then decreased with a further increase in the Si/Al ratio.[201] More investigations revealed that the strength of the BASs in the 8MR side pockets of **MOR** zeolite decreased with an increase in Si/Al ratios[202] and the catalytic performance of **MOR** zeolites on DME carbonylation is mainly determined by the BASs in the 8MR channels.[141,201–203]

The conversion of methanol to hydrocarbons (MTH) catalysed by zeolites including methanol to olefins (MTO), methanol to propane (MTP), methanol to gasoline (MTG), and methanol to aromatics (MTA) provides an alternative route for producing basic chemicals on a large scale from non-petroleum sources. However, there is a debate on the aromatic-based hydrocarbon pool (HCP) mechanism and the olefin methylation/cracking mechanism.[204–206] Because MTH reactions are catalysed by BASs, the Si/Al ratios of zeolites will definitely affect their catalytic performance. For example, Guisnet and co-workers explained that a lower Si/Al ratio of a zeolite results in a higher density of acid sites; thus a larger number of successive chemical steps occurred along the diffusion path within the zeolite, which favours the condensation reactions and leads to a faster coking rate.[207,208] In the MTH reaction catalysed by Beta zeolite, propylene selectivity increased from 50.2% to 60.8% and aromatic selectivity decreased from 3% to 0.3% when the Si/Al ratio was increased to 300 from 150.[49] As expected, high-silica ZSM-5 (Si/Al = 181) with low acid density exhibited outstanding catalytic performance in the MTP reaction.[77] Moreover, the low acid density due to the high Si/Al ratio prolongs the catalytic lifetime of zeolites in MTH. In the MTO reaction catalysed by H-ZSM-5 and H-ZSM-11 with different Si/Al ratios, the catalytic lifetime increases with increasing the Si/Al ratio due to the low acid density which reduces condensation reactions.[209] Liu and co-workers reported that the hierarchical Beta zeolite with a low acid density (Si/Al = 277) showed a much longer catalytic lifetime and slower coking rate in the MTO reaction than the non-hierarchical Beta zeolite with conventional acid density (Si/Al = 228).[80]

Beta zeolite is a newly developed catalyst for converting aqueous lactic acid (LA) to lactide (LT), a key building block toward a biodegradable and renewable polylactic acid (PLA).[210] Yu and co-workers synthesized nanosized Beta zeolites with a Si/Al ratio of 15.5 and nanosized hierarchical Beta zeolite with a Si/Al ratio of 10, which exhibited outstanding LT yields of 74.0% and 77.5%, respectively.[75,211] These results suggest that the high density of Brönsted acid sites with better accessibility favours the conversion of LA to LT.

2.4.2. Adsorption/separation. Because of their well-defined microporous structures, BASs, and compensated cations, zeolites are widely employed for gas drying, air separation, hydrogen purification, separation of paraffin isomers, xylene isomers, inert gases, and light hydrocarbons, capture and separation of carbon dioxide, storage of methane and hydrogen, and removal of harmful gases.[7] In the framework of zeolites, the proton attached to the O atom linking the Al and Si atoms has an intrinsic affinity to water.

Zeolites are one of the most commonly employed adsorbents in the temperature swing adsorption (TSA) process for natural gas drying. The affinity of protonic zeolites to water is mainly driven by the intrinsic attraction between the polar molecules and the BASs by dipole-field interaction. Furthermore, the presence of cations enhances the affinity of zeolites to polar adsorbate molecules. Thus, the Si/Al ratios of both cationic and protonic zeolites have a significant influence on water adsorption.[164,212] The higher the content of Al in the framework, the more cations are required to balance the charge and thus higher water uptake is expected.[164] For example, Na^+ balanced **CHA** zeolite with a Si/Al ratio of 2 exhibited a significant adsorption capacity for water. However, dealuminated Y zeolite with a Si/Al ratio of >200 is highly hydrophobic.[113,164]

Unlike the adsorption of polar H_2O in zeolites, air separation by zeolites relies on the difference in the stronger quadrupole interaction between the cations and N_2 *versus* O_2.[213,214] Thus, a zeolite with a large capacity of cations would be beneficial for air separation. As expected, Al-rich zeolites were used for air separation such as low-silica X (LSX, Si/Al = 1)[215–217] and ZSM-2 (Si/Al = 1.6).[218] Recently, Al-rich **CHA** (Si/Al = 1.6–2.0) was prepared and exchanged with Li^+ for N_2 adsorption.[58]

The strong local electric field and high basicity of the framework of zeolites cause a strong interaction with acidic CO_2 molecules. Al-rich zeolite such as NaLSX with a Si/Al ratio of 1 is a typical CO_2 adsorbent.[219,220] The affinity to CO_2 increases along with a decrease in Si/Al ratios.[221] For example, Na-type ZSM-5 with lower Si/Al ratios exhibited a higher affinity to CO_2.[222] Corma and co-workers reported that the interaction between the adsorbed CO_2 molecules and the framework of the **LTA** zeolite increased with the increase of the Al content.[15] Wang and co-workers studied the $CO_2/CH_4/N_2$ adsorptive separation by **CHA** zeolites with various Si/Al ratios and discovered that the higher Si/Al ratios result in weaker electrostatic fields and the separation performance for both CO_2/CH_4 and CO_2/N_2 decreases with an increase in Si/Al ratios, while the regeneration capacity of CO_2 presented an opposite trend because the polarity of CO_2 is higher than that of CH_4 and N_2, and thus the interaction between CO_2 molecules and the **CHA** framework is more sensitive to the variation of the electrostatic field, *i.e.*, the Si/Al ratio.[223] However, the high content of Al with a large number of extra-framework cations near the windows of pores might lead to poor capacity for the adsorbates. For example, Na-type GIS zeolites with a Si/Al ratio under 2.2 showed less CO_2 uptake ($\leq$0.7 mmol g^{-1} at 25 °C and 1.0 bar) than those with a Si/Al ratio from 2.5 to 4.7 due to the large number of cations near the 8-ring windows.[224]

Coal bed methane (CBM) is an unconventional gas with a main composition of CH_4, N_2, and CO_2. Separation of methane has important economic value and environmental significance, which requires the selective capture of CH_4 from N_2 and CO_2. CH_4 and N_2 have very similar dynamic molecular diameters and thus the enrichment of CH_4 from CBM mainly depends on their difference in polarizability. Compared to N_2, CH_4 has higher polarizability and thus a higher affinity towards polar surfaces. For example, **FAU** zeolite is a common and efficient adsorbent for the adsorption of CH_4 from N_2 due to its high polar surface, high specific surface area, and large pore volume.[225,226] Azizpour and co-workers studied the influence of the Si/Al ratios in the **FAU** zeolite on the adsorption of CH_4 and N_2 and discovered that the adsorption capacity towards CH_4 was improved by decreasing the Si/Al ratios because of the formation of more acid sites in the Al-rich **FAU** zeolite.[227]

As mentioned above, high-silica zeolite is hydrophobic and has the ability to adsorb organic compounds.[228] For example, ZSM-5 zeolite has the ability to adsorb methyl *tert*-butyl ether (MTBE) from water and the distribution coefficient K_d is improved by increasing the Si/Al ratios.[229] Because zeolites have a negative framework, only neutral or positive organic compounds in water can be adsorbed by zeolites. For example, ZSM-5 (Si/Al = 80) and **MOR** (Si/Al = 200) zeolites both showed high removal ability for neutral and positive nitrosamines in demineralized water.[230] However, negative organic compounds can also be adsorbed by zeolites if they can be protonated in solution. For example, rhodamine B (RB) molecules can be protonated in the solution with a pH < 3 and can be adsorbed by Beta zeolite.[231] If the pH of the solution is greater than 3, RB converts to a zwitterionic form which causes an electrostatic repulsion between the RB molecules and the Beta zeolite. By increasing the Si/Al ratios of Beta zeolite, the adsorption capacity for RB increases and reaches a maximum value of 4.808 mg g^{-1} at Si/Al = 9.2.[231]

In the adsorption of organic compounds from solution by zeolites, solvent molecules will be competitively adsorbed. For example, Jiang and co-workers studied the adsorption of 2,4,6-trichlorophenol (TCP) by high-silica **FAU**.[232,233] It was observed that a supercage accommodated approximately 2 TCP molecules in an Al containing cage and 2.5 TCP molecules in a non-Al containing cage because Al-containing cages adsorbed more water molecules than the cages without Al (Fig. 7), illustrating an increase in the adsorption capacity of **FAU** zeolite for TCP along with an increase in the Si/Al ratios.[232,233]

Zeolites can also be used for hydrogen storage because of their BASs and the electrostatic field within the channels or cages. In 1998, a study on H_2 adsorption at 77 K on NaX zeolites with various Si/Al ratios indicated that the H_2 adsorption capacity on NaX zeolite with low Si/Al ratios is larger than that on the NaX zeolite with high Si/Al ratios.[234] Later, Chang and co-workers reported that the isosteric heat of H_2 adsorption increased with a decrease in Si/Al ratios.[235] As expected, the Al-rich **CHA** zeolite and low-silica X fully exchanged by alkali-metal cations also showed good potential for H_2 adsorption.[236,237]

2.4.3. Ion-exchange. According to the origin of the negative charge of zeolites, the Si/Al ratio of a zeolite will certainly affect the cationic exchange capacity and the location as well as the state of the compensating cations. In principle, a low Si/Al ratio corresponds to a high ion-exchange capacity and the maximum ion-exchange capacity is achieved when the Si/Al ratio of a zeolite is 1.[238] For example, the Ag^+ exchange capacity of **FAU** zeolite with a Si/Al ratio of 2.5 is much higher than that of **FAU** zeolite with a Si/Al ratio of 40.[239] A zeolite with a low Si/Al ratio possesses a high ion-exchange capacity and therefore facilitates the application in water softening and heavy metal cation removal from water.[240] Moreover, the Si/Al ratio of a zeolite can also affect the ion-exchange selectivity. For example, a zeolite with a high Si/Al ratio results in a low anionic field that gives rise to an enhanced selectivity towards monovalent cations,[241] while zeolites with a Si/Al ratio of around 1 are highly selective for divalent cations.[238] In zeolites with low Al content, the hydration energy is the major factor contributing to selectivity. An ion with higher (negative) hydration energy is preferentially ion-exchanged.[242] The selectivity follows the order of $Cs^+ > Rb^+ > K^+ > Na^+ > Li^+$. As the Al content increases, the contribution of electrostatic attraction is the major factor for the selectivity and the selectivity is reversed to $Na^+ > Li^+ > K^+ > Rb^+ > Cs^+$. Furthermore, high-silica zeolites prefer univalent cations such as alkali ions and NH_4^+.[242,243]

3. Regulation of Al distributions of zeolites

Because of the strong electromagnetic interaction between the positive charge of the cations and the negative charge of the O near Al, it is expected that the Al distributions of zeolites can be regulated during the synthesis by selecting organic or inorganic SDAs with a specific configuration.[244–247] According to the formation process of zeolites, changing the Si/Al ratios of aluminosilicate oligomers can also regulate the Al distributions in the framework of a zeolite.[248,249] In addition, the tension of the tetrahedral sites (T-sites) in the framework of a zeolite usually depends on its position. Thus, the removal of Si or Al with high tension *via* "post-synthesis" or "post-treatment" can also be used to regulate Al distributions.[184]

According to the origin of Brönsted acidity, the Al distributions in zeolites decide the strength and distributions of BASs and further affect their performance in catalysis, adsorption/separation, and ion-exchange. Basically, the distribution of Al in the framework of a zeolite has three situations: (i) the location of Al atoms at/within the individual crystallographically distinguishable framework T sites; (ii) the spatial correlation of two or more Al atoms, *i.e.*, the distances and the possibility of neighbouring Al atoms cooperating in the formation of active sites; and (iii) the external surface, internal channels, or intersections, as shown in Fig. 8.[248] Regulating and determining the distributions of Al atoms in the framework of a zeolite is extremely microscopic and challenging. In general, there are "bottom-up" and "up-bottom" strategies to approach the regulation of Al distributions.

3.1. "Bottom-up" tuning of the Al distributions of zeolites

The "bottom-up" strategy for tuning the Al distributions of zeolites is mostly performed by changing the components of the initial mixture or the synthesis conditions. The location of Al in the framework of zeolites is related to the intrinsic thermodynamic stability of Al at different T sites and the kinetic factors in gelation and crystallization processes, which include the coordination structure of Al species, Si/Al ratios, OSDAs, cations, and the nature of raw materials.

Al distributions are closely associated with the Si/Al ratios of the framework of a zeolite. For example, it was reported that the proportion of the Al atoms sitting at the intersections of H-**MFI** zeolite, especially for the Al pairs, increased with a decrease in the Si/Al ratios.[250] As for zeolites, there are several types of Al distributions that have been identified: (i) Al–O–Si–O–Al sequences in low silica zeolites, for example in **CHA** zeolite with a Si/Al ratio below 7,[251] in Beta zeolite with a Si/Al ratio of 4.5,[252] and in A zeolite with a Si/Al ratio of 1/1; (ii) Al–O–$(Si–O)_2$–Al or Al–O–$(Si–O)_3$–Al sequences in the rings forming cationic sites for bare divalent cations such as Co^{2+} (denoted as Al pairs); (iii) Al–O–$(Si–O)_{n\geq 2}$–Al sequences accommodating Co^{2+} hexaaqua complexes in hydrated zeolites, but not bare Co^{2+} in dehydrated zeolites (denoted as close unpaired Al atoms); and (iv) Al–O–$(Si–O)_{>3}$–Al sequences with far distant Al atoms located in different rings which are unable to accommodate both bare Co^{2+} and Co^{2+} hexaaqua complexes (denoted as single Al atoms).[249,253] The close unpaired Al atoms have been identified in SSZ-13, Beta, and ZSM-5 zeolites now.[252–254]

As for the **MFI** zeolite, the Al atoms in Al-rich ZSM-5 with a Si/Al of < 10 are predominantly present in the form of Al–O–Si–O–Al sequences.[248,255] When the Si/Al ratio of ZSM-5 increases, the relative concentration of Al pairs decreases, while the relative concentration of single Al atoms increases.[256] As for silica-rich **FER** zeolites (Si/Al = 20, 27, 30), the framework contains only isolated Al atoms, while for Al-rich **FER** zeolites (Si/Al = 8.6 and 10.8), the framework contains Al–O–$(Si–O)_2$–Al sequences.[249] Unlike **MFI** and **FER** zeolites, Al atoms are more easily distributed in the diagonal position of the 4-ring of the **FAU** zeolite (Y zeolite, Si/Al = 15, 11, 8.6, 7, 5.8), as confirmed using the density functional theory (DFT) calculations. With the decrease of the Si/Al ratio from 15.0 to 5.8, the Al atoms are, prior to distribution, in the form of a trigonal symmetrical arrangement around the same Si atom.[257] While Si-rich ***BEA** (Si/Al > 12) zeolites do

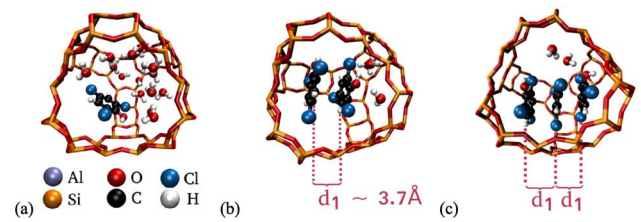

Fig. 7 Arrangements of TCP and water molecules in the non-Al containing supercages of **FAU**250 (Si/Al ratio in the simulated box is 255) zeolites: (a) 1 TCP, (b) 2 TCP, and (c) 3 TCP molecule(s) per cage at TCP equilibrium concentrations equal to (a) 4.6, (b) 77.6 and (c) 77.6 μmol L^{-1}. The characteristic distance between the center of mass of the benzene rings in the TCP molecules is shown as d_1. Reproduced from ref. 232 with permission from Elsevier, Copyright 2020.

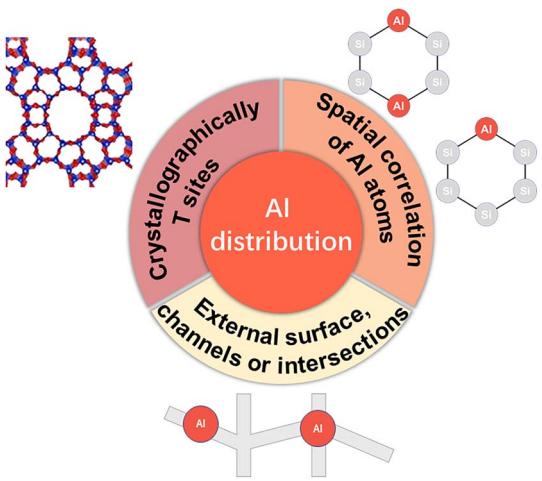

Fig. 8 Three situations of Al distribution: (i) the location of Al atoms at/within the individual and crystallographically distinguishable framework T sites; (ii) the spatial correlation of two or more Al atoms, *i.e.*, the distances and the possibility of neighbouring Al atoms cooperating in the formation of active sites; and (iii) the external surface, internal channels, or intersections.

not contain Al–O–Si–O–Al sequences, Al-rich ***BEA** (Si/Al = 4–5) zeolites contain Al atoms in the form of Al–O–Si–O–Al sequences with concentrations in the range from 40% to 100% of the total Al and the most populated (50–65%) Al atoms are the unpaired Al atoms located in different rings of the channel surface.[252] However, regardless of the types of zeolites, the presence of Al–O–$(Si–O)_2$–Al sequences in the zeolite framework is a key feature of high-silica zeolites even when Si/Al is relatively high (>25).[249]

SDAs including OSDAs and alkali metal cations (*e.g.*, Na^+) have a great influence on the Al distribution in the framework of zeolites because the Al species are located near the SDAs to balance the positive charge (*vice versa*). In the ZSM-5 zeolite with a Si/Al of > 10, the Al pairs in close vicinity to quaternary N atoms of TPA^+ are mostly located in β-type 6MRs at the intersection of straight and sinusoidal channels.[258] The pre-organized organic–inorganic composites around TPA^+ (*i.e.*, oligomers) control the distribution of Al atoms in the framework of ZSM-5; that is to say, SDAs, especially OSDAs with specific structures affect the numbers of Al atoms incorporating the framework of zeolites and thus the Al distributions of Al atoms in the framework of zeolites.[258] For example, the Al atoms in ZSM-5 zeolite synthesized with TPA^+ in the absence of Na^+ are predominantly located at channel intersections, while the Al atoms in the ZSM-5 zeolite synthesized with both TPA^+ and Na^+ are located not only at the intersections but also in narrow straight and sinusoidal channels because TPA^+ is exclusively located at the intersections and Na^+ is located within the channels.[259] In the synthesis of ZSM-11 zeolite, the addition of Na^+ or Li^+ to the initial synthesis mixture can increase the proportion of the Al atoms at the intersection cavity of ZSM-11.[246] Besides, the introduction of Na^+ in the initial synthesis mixture can also induce the migration of Al atoms from the straight channel to the intersection cavity. In the absence of alkali metal ions, increasing the Si/Al ratios of the framework leads to a more prominent decrease of the Al atoms in the intersection cavity and a relative enrichment of the Al atoms in the straight channel. Introducing alcohols as a pore-filling agent in the synthesis of zeolites creates an Al free environment around the alcohol molecule because of the neutral nature of alcohol molecules. For example, the Al atoms in the ZSM-5 zeolite are preferentially located in the narrow straight and sinusoidal channels instead of at the intersections if the bulky and branched-chain alcohols, such as pentaerythritol (PET) and trimethylolethane (TME) are used as additives.[245,260,261]

As mentioned above, an OSDA affects the Al distributions in the framework of zeolites *via* (1) a strong interaction between the organic cation and the framework oxygen atoms surrounding Al ($SDA^+\cdots OAl^-$) and (2) occupying the well-defined positions within the void volume of the framework structure. Thus, it is expected that the Al distribution is determined by the location of the SDA species within the zeolite framework during synthesis.[262] For example, Okubo and co-workers reported that the occupancy of Al atoms at different T sites in **IFR** zeolites can be tuned by selecting appropriate OSDAs.[263] In the framework of **MOR** zeolite synthesized with hexamethyleneimine (HMI) and Na^+ as the SDAs, the BASs are enriched in the 8MR channels even at a low Al content in the zeolite framework (*i.e.*, a high Si/Al ratio) because the HMI molecule (kinetic diameter, 0.76 nm) can only be accommodated in the 12MR pores, driving Na^+ into the 8MR channels and thus enriching the Al atoms in the 8MR channels.[201,264] Pinar and co-workers also regulated the Al distribution in **FER** zeolite directed by TMA^+ by introducing the second OSDA, pyrrolidine, which has a stronger interaction with the framework than TMA^+ and thus prohibits the incorporation of Al atoms into specific positions.[262] Tatsumi and co-workers synthesized **RTH**-type zeolites in the absence/presence of OSDAs.[265] When large OSDA molecules such as 1,2,2,6,6-pentamethylpiperidine (PMP) and *N*-methyl-piperidine (MP) are used as OSDAs, they are preferentially located in the large non-distorted 8MR pores rather than the distorted 8MR ones, which makes the Al atoms preferentially incorporate into T_1 and T_2 sites but not the T_3 site because the T_3 site does not face any 8MR pores. In contrast, in the OSDA-free synthesis of **RTH**, the Al atoms could be uniformly distributed at the T_1, T_2, T_3, and T_4 sites because they are accompanied only by Na^+. When pyridine (Py) with a size smaller than PMP and MP but larger than Na^+ was used as the OSDA, more Al atoms are incorporated into the T_4 site located at the distorted 8MR pores.[265] Moreover, the size of the alkali metal ions may also affect the Al distributions. For example, Fan and co-workers discovered that the proportion of the paired Al atoms in the total Al species in SSZ-13 decreased to 44%, 28%, 16%, and 10% with increasing the radii of alkali metal ions Li^+, Na^+, K^+, and Cs^+, respectively.[266] In this case, small rings such as double-six-membered rings (D6Rs) can accommodate only small alkali metal cations Li^+ and Na^+ instead of large alkali metal cations K^+ and Cs^+. Thus, Li^+ and Na^+ directed more Al atoms into small D6Rs, which accounted for the high content of paired Al species in the resultant SSZ-13.

Considering that the location of the Al atoms in the framework of zeolites can be affected by the size of both OSDAs and alkali metal ions, the Al atoms at specific positions of the framework thus can be regulated by combining OSDAs and alkali metal ions. For example, the SSZ-13 zeolites (Si/Al = 15–30) synthesized in the presence of $TMAda^+$ cations did not contain any paired Al sites, while introducing Na^+ promoted the formation of paired Al sites and a linear relationship between the number of paired Al sites and the $Na^+/TMAda^+$ ratio (0–1) was observed.[163] The proportion of paired Al reached the maximum at a $Na^+/TMAda^+$ ratio of 1 and decreased as the $Na^+/TMAda^+$ ratio was between 1 and 2.[163] Schneider and co-workers reported that the **CHA** zeolite directed by (a) $TMAda^+$ only; (b) the combination of $TMAda^+$ and Na^+; and (c) the combination of $TMAda^+$ and K^+ contained (i) one $TMAda^+$ in each cage; (ii) one $TMAda^+$ in each cage and Na^+ in the 6MR in an amount linearly proportional to the amount of the paired Al sites in 6MR; and (iii) one $TMAda^+/K^+$ in each cage (Fig. 9), corresponding to isolated, paired, and isolated Al, respectively.[267] Moreover, the type of OSDA (*i.e.*, HMI or cyclohexylamine) occluded in the MCM-49 zeolite also has a significant impact on Al distributions. When HMI was used as the OSDA, the Al distribution at the T sites in MCM-49 followed the ratio of $T_2 : (T_1, T_3, T_4, T_5, T_8) : (T_6, T_7) = 19 : 69 : 12$, while this ratio shifted to $T_2 : (T_1, T_3,$

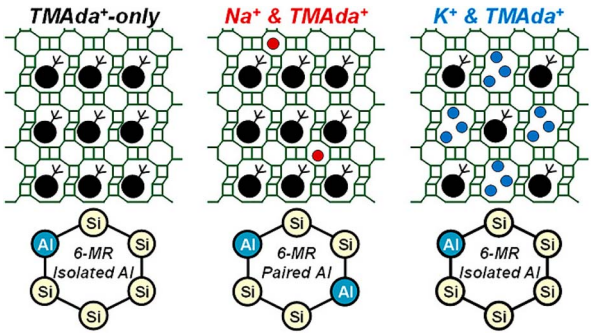

Fig. 9 Cooperation or competition between organic and inorganic SDAs for Al distributions of **CHA** zeolites. Reproduced from ref. 267 with permission from the American Chemical Society, Copyright 2020.

T_4, T_5, T_8) : (T_6, T_7) = 32 : 63 : 5 when cyclohexylamine was used as the OSDA.[244]

Introducing trivalent or tetravalent heteroatoms such as B and Sn into the framework of a zeolite to competitively occupy various T sites with Al atoms is also a feasible route for regulating Al distributions. For example, the Al distribution among the three types of pores in MCM-22 can be regulated by adjusting the content of B incorporated during the synthesis.[268] With a proper content of B, BASs can be enriched in the sinusoidal channels rather than in the surface pockets and the supercages. When the B/Al ratio in the initial mixture (Si/Al = 200) reaches 7 or 9, the Al content in the narrow straight/sinusoidal channels is increased.[26] In the framework of ZSM-5, B atoms preferentially occupy the positions at the intersections, which enriches the Al atoms in the 10MR channels.[269] Moreover, introducing Sn into the framework of ZSM-5 leads to the preferential location of Al atoms in the straight channels rather than at the intersections.[28] Recently, Shen and co-workers reported that introducing Mg into the framework of ZSM-5 results in a slight increase in the amount of Al pairs in both the straight channel (from 5% to 10%) and the sinusoidal channel (from 16% to 22%).[270]

Besides regulating the interaction between the SDA and oligomers, modifying the Al distributions in the oligomers can also alter the Al distributions of the resultant zeolites. For instance, changing the nature of the source materials can also modify the Al distributions in the framework of zeolites. Preferential Al distribution in the narrow straight/sinusoidal channels of ZSM-5 is observed when silica sol is the Si source, while the Al atoms are enriched in larger channel intersections when tetraethyl orthosilicate (TEOS) is used as the Si source.[29] Compared to the Al source $Al(NO_3)_3$ and Al-tri-*sec*-butoxide, the Al source $AlCl_3$ or $Al(OH)_3$ resulted in a significant increase in the amount of Al–O–$(Si–O)_{1,2}$-Al sequences in the same ring of ZSM-5 (<10% for $Al(NO_3)_3$ and Al-tri-*sec*-butoxide, 33% for $AlCl_3$ and 27% for $Al(OH)_3$).[254,271] In the interzeolite transformation synthesis, the Al distribution in the resultant zeolite is usually different from that formed by the direct hydrothermal synthesis. For example, the **CHA** zeolite from the interzeolite conversion of **FAU** zeolite contains more Al pairs than the **CHA** zeolite from the direct hydrothermal synthesis.[272,273] Recently, Yabushita and co-workers synthesized Al-pair-rich **CHA** zeolites by using lab-made Al-rich amorphous aluminosilicate containing a large quantity of Al–O–Si–O–Al sequences as the source material.[274] Besides cations, halogen anions can also affect the Al location by interacting with SDAs and oligomers.[275,276] For example, Cl^- anions can induce more Al atoms to sit on the external surface of ZSM-11 crystals while larger Br^- or I^- anions lead to a uniform distribution of Al species in the inner straight channels.[275] Furthermore, the crystallization temperature also has an impact on Al distributions. For example, ZSM-5 obtained at 230 °C exhibits a higher proportion of Al pairs at the intersections than ZSM-5 obtained at 120 °C because the Al substitution at the channel intersection, which competes with the substitution in the straight channel, becomes more feasible at elevated temperature.[27]

3.2. "Top-down" tuning of the Al distributions of zeolites

As mentioned above, dealumination can selectively remove the Al atoms at specific sites, which can tune the Al distributions in the framework of zeolite. For example, Lercher and co-workers investigated the Al distributions of Beta zeolites with Si/Al = 12.5 (HBEA25) and Si/Al = 75 (HBEA150) dealuminated *via* leaching with extended X-ray absorption fine structure (EXAFS) and ^{27}Al MAS NMR.[277] The results indicated that the distribution of Al T-sites in HBEA150 is significantly different from those in HBEA25. HBEA150 has a lack of population in T_7 and T_2 sites, which are highly populated in HBEA25. The resilience of the T_5 and T_6 sites toward the removal of Al is also observed. In the framework of ZSM-5, the Al atoms in straight and sinusoidal-shaped channels are more stable than those at the intersections toward steam treatment at high temperatures.[278] Shen and co-workers reported a mild-acid-assisted thermal/hydrothermal dealumination method for Beta zeolite.[184] In such a study, Beta zeolite was first steamed, which eliminated most of the framework Al, especially Al atoms at the T_2, T_5, T_6, and T_7 sites. In the subsequent acid-calcination treatment, the extra-framework Al (EFAL) and the framework Al in the defect sites, especially the Al at T_5, T_6, and T_9 sites, are removed. Very recently, Liu and co-workers developed a low-pressure $SiCl_4$ treatment (LPST) strategy to replace the framework Al atoms at the T_1, T_2, and T_4 sites of the 12MR channels of **MOR** zeolite and discovered that the resultant $AlCl_3$ species migrate into the 8MR channels and directly reinsert into the T_3 sites as a new framework Al through the reaction between $AlCl_3$ and silanol defects (Fig. 10).[203]

3.3. Methods for determining the Al distributions of zeolites

Chemical environments of Al atoms are diverse and complex which are affected by the topology of zeolites; therefore an unambiguous determination of the Al distributions in the framework of zeolites is challenging.

So far, solid-state ^{27}Al MAS NMR has been the main technique to determine the Al distributions in the framework of high-silica zeolites, which is sensitive to the local environments of the Al atoms in the framework of zeolites and is in principle capable of distinguishing between ^{27}Al species at different T

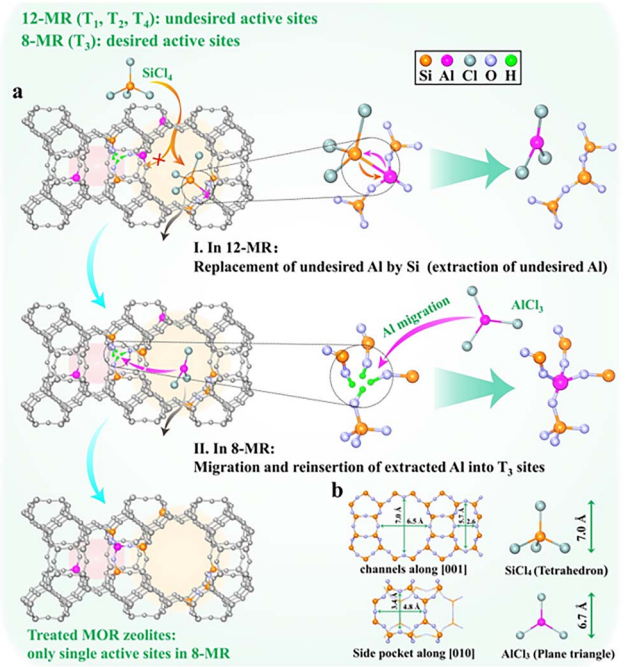

Fig. 10 (a) Schematic of a typical treatment process, showing the directional migration of framework Al into T_3 sites of the **MOR** zeolite *via* LPST. (b) Topology of **MOR** and steric configuration of $SiCl_4$ and $AlCl_3$ molecules with a kinetic diameter of 7.0 and 6.7 Å, respectively. Reproduced from ref. 203 with permission from Wiley, Copyright 2022.

sites.[279] However, due to the strong quadrupolar interactions of ^{27}Al (I = 5/2) nuclei and the inhomogeneous distributions of ^{27}Al species, the resolution of the ^{27}Al MAS NMR spectra is limited and can only show whether the Al site is in the framework (tetrahedral) or the extra-framework Al (octahedral).[280,281] Several advanced ^{27}Al MAS NMR techniques have been developed to improve the resolution of the NMR spectra, such as using higher magnetic fields (>18 T), multiple-quantum magic angle spinning (MQMAS), and multidimensional NMR.[282] By applying these techniques, new information about the Al sites in the framework of zeolites has been obtained. For example, high-field ^{27}Al MQMAS NMR analyses of different ZSM-5 zeolites allowed the identification and assignment of at least 12 different ^{27}Al signals associated with different T sites.[278,283] MQ NMR spectra collected at 18.8 T revealed four non-equivalent T-sites of **MOR** zeolites.[203] Furthermore, the 2D (two-dimensional) ^{29}Si–^{27}Al D-HMQC (dipolar-mediated heteronuclear multiple-quantum coherence) spectrum was employed to investigate the Al incorporation in the crystallization of MCM-49 (**MWW**-type) and ZSM-5 zeolites.[73,284] Moreover, the ^{27}Al MAS NMR spectra acquired at 18.8 T and ^{13}C{^{27}Al}/^{1}H{^{23}Na} REAPDOR (rotational echo adiabatic passage double resonance) MAS NMR, 2D ^{27}Al 3Q (triple quantum) MAS, ^{1}H–^{13}C HETCOR (heteronuclear correlation) MAS, and ^{1}H–^{27}Al/^{1}H–^{23}Na D-RINEPT (dipolar refocused-insensitive nuclei enhancement by polarization transfer, INEPT) MAS NMR experiments were employed to analyses the Al distributions in MCM-49 zeolite with different OSDAs.[244] 2D ^{27}Al MQMAS NMR spectra were used to determine the Al sites in ZSM-11 zeolite and four signals were distinguished.[246] 2D ^{27}Al 3QMAS NMR was used to analyse **IFR** zeolite and distinguished four resonances that presumably corresponded to the different Al locations at four T sites in **IFR** zeolite, which can suppress and correctly deal with the quadrupolar effect of ^{27}Al.[263]

Recently, Bokhoven and co-workers exploited the resonant (anomalous) scattering near the Al K edge (1.56 keV or 7.95 Å) to obtain a quantitative assignment of Al to the T sites in a zeolite framework.[285] By combining the conventional X-ray powder diffraction data collected at the Al K edge, the distribution of Al over the T sites in a zeolite framework structure can be determined quantitatively and unambiguously. This method can be applied even to zeolites with Si/Al ratios as high as 15.

Techniques such as XRD and NMR mainly offer bulk average of the information of a specific sample. Although a number of tomographic techniques have been developed to give 3D reconstructions, none of them currently offer sub-nanometer spatial resolution.[286] These techniques also have difficulty differentiating the primary elements consisting of zeolites (*i.e.*, Al, P, and Si) due to their close and light atomic masses. However, atom probe tomography (APT) can provide three-dimensional compositional mapping with sub-nanometre resolution and sensitivity in the range of parts per million (ppm) for all elements.[287] For example, Weckhuysen and co-workers employed APT to determine the Al distributions of zeolites (Fig. 11).[286,288,289] It is shown that Al atoms are non-randomly distributed within the ZSM-5 crystals with a most probable Al–Al neighbour distance of 18 ± 6 Å, an average Al density of 0.025 atoms per nm^3, and a relative strength of non-randomness of 0.7. Because there are 12 and 24 crystallographically distinguishable framework T sites in the **MFI** structure with symmetry of *Pnma* and $P2_1/n$, respectively, the current results suggested that the Al atoms preferentially locate at some crystallographically distinguishable framework T sites in ZSM-5 crystals due to the preference of thermodynamics. In severely steam-treated ZSM-5 crystals, they found that the Al distribution is also non-random. However, such a technique can only provide local information, beyond the concept of distribution in topology.

Labelling can be employed to determine Al distributions indirectly. Molecules such as carbon monoxide (CO), Py, and 2,6-di-*tert*-butylpyridine (DTBPy) can be used as probes of the acid site location.[290,291] The probe molecules with different sizes could be adsorbed on different accessible acid sites, which can be further characterized by FT-IR or ^{13}C NMR and thus reveal the Al distributions.[291] Moreover, certain divalent cations such as Co^{2+} are practical experimental probes for paired Al in zeolites because single Al atoms cannot accommodate Co^{2+} while Al pairs can accommodate bare Co^{2+} and hydrated Co^{2+} and close unpaired Al can only accommodate hydrated Co^{2+}. For example, with this method, the amount of single Al atoms, Al pairs, and close unpaired Al atoms in SSZ-13 can be calculated as follows:

$$[Al_{single}] = [Al_{framework}] - 2[Co_{max}] \quad (4)$$

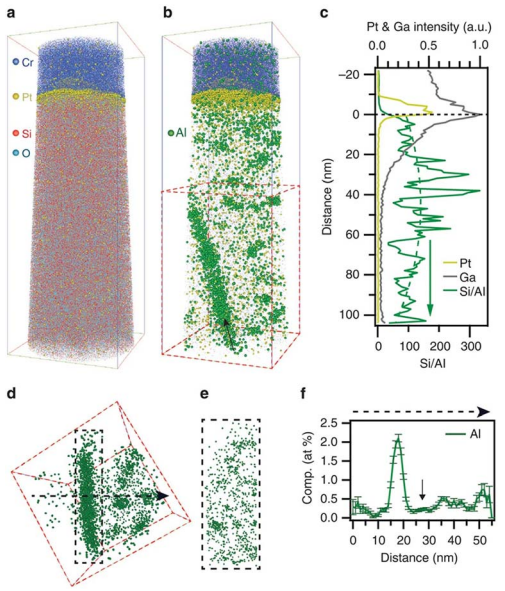

Fig. 11 (a) Si and O and (b) Al atom distributions from within a steam-treated zeolite ZSM-5 crystal. The Cr and Pt layers serve as a fiducial marker to mark the position of the zeolite crystal surface. Bounding box dimensions are 46 × 45 × 126 nm^3. (c) Si/Al ratio as a function of distance from the surface marked by a black dashed line. A least-squares polynomial fit is shown as a green dotted curve to guide the eye to the distribution. The Pt and Ga intensities as well as the Si/Al ratio values are averaged over each cross-section when moving from the top to the bottom of the analysed volume. (d) Al distribution of isolated subvolume (red dashed box) viewed normal to the arrow direction in (b). Bounding box dimensions 53 × 58 nm^2. (e) Plane view of the isolated subvolume outlined by the dashed box in (d). Bounding box dimensions 26 × 67 nm^2. (f) 1D composition profile with associated error bars taken across the arrowed black dashed line in (d). Reproduced from ref. 288 with permission from Springer Nature, Copyright 2015.

$$[\mathrm{Al_{pair}}] = 2([\mathrm{Co_{bare}}] - [\mathrm{Co_{D6R}}]) \quad (5)$$

$$[\mathrm{Al_{close}}] = 2[\mathrm{Co_{max}}] - 2([\mathrm{Co_{bare}}] - [\mathrm{Co_{D6R}}]) \quad (6)$$

where $[\mathrm{Co_{max}}]$ is the Co concentration in the zeolite maximally exchanged by the Co^{2+} hexaaqua complex, $[\mathrm{Co_{bare}}]$ is the concentration of bare Co^{2+} in the maximally bare Co^{2+} exchanged zeolite, and $[\mathrm{Co_{D6R}}]$ is the concentration of bare Co^{2+} in the hexagonal prism.[248,253,292] This method has been successfully used for determination of Al pairs in **CHA**, **MFI**, and **MEL**.[27,245,246,267,292,293] Co^{2+}-type zeolites can also be studied by UV-vis spectroscopy in which bands in the UV-vis spectra correspond to the Co^{2+} ions coordinated to the Al atoms at different positions.[209] The role of ion-exchanged Cu^{2+} is similar to that of Co^{2+} but more sensitive to the conditions.[248] Upon ion-exchange, the Cu^{2+} species compensate for the negative charge of the framework and the formation of Cu-complexes simply depends on the location of the Al atoms. Besides Co^{2+} and Cu^{2+}, Mo species can also be used to distinguish Al atoms from Si atoms because the Mo species have strong interaction with Al atoms and the Mo species can be determined from the atomic-resolution transmission electron microscope (TEM) images

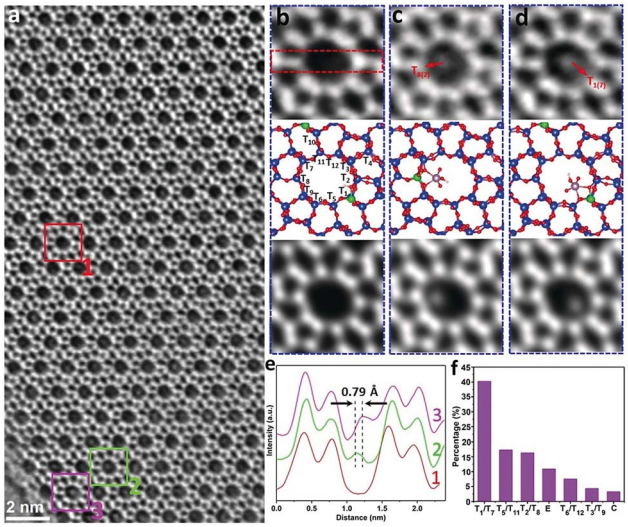

Fig. 12 (a) A representative integrated differential phase-contrast scanning transmission electron microscopy (iDPC-STEM) image of Mo/ZSM-5, showing the presence of off-center contrast in many 10MR channels. (b–d) Zoomed-in areas 1, 2, and 3 of (a), respectively, corresponding to three scenarios: an empty channel (b), and channels containing a MoO_3H cluster bound at the T_8 site (c) and at the T_1 site (d). Each panel includes the raw image (top), the calculated structural model (middle), and the simulated projected electrostatic potential (bottom). Si: blue, O: red, Al: green, Mo: pink, and H: white. (e) Intensity line profiles of the images in (b)–(d), across the areas as represented by the red dashed rectangle. (f) Statistics of Al occupancy at different T sites, based on the results of one hundred channels. The labels "E" and "C" represent empty channels and channels with an on-center extra contrast, respectively. Reproduced from ref. 294 with permission from Wiley, Copyright 2019.

(Fig. 12).[294] In addition, CO_2 can also be used to probe the location of Al atoms in the framework of zeolites.[295] Recently, Chiesa and co-workers reported that paramagnetic Zn^I is also a convenient spin label that can be used to determine the Al distributions within the framework of a zeolite by pulse dipolar spectroscopy (PDS).[31]

3.4. Impact of Al distributions on the performance of zeolites

For a given zeolite, the performance of catalysis, adsorption-separation, and ion-exchange is significantly affected not only by Si/Al ratios but also by Al distributions.

3.4.1. Catalysis. In catalytic cracking, BASs are the active sites. Thus, the activity and selectivity depend on the Al distributions in the framework of zeolites. For example, Beta zeolites with selectively removed Al atoms on T_5, T_6, and T_9 sites show a higher gasoline yield, while those with selectively removed Al atoms at the T_2, T_5, T_6, and T_7 sites show a higher diesel yield in vacuum gas oil (VGO) catalytic cracking.[184] In the catalytic cracking of 1-octene over ZSM-5 zeolite, the acid sites at the intersections have a positive contribution to the bimolecular reactions involving carbenium cations and olefins.[296] Cracking of *n*-hexane over ZSM-5 exhibits a similar trend. The acid sites at the intersections and/or external surfaces enhance the

formation of aromatics and coke.[260] Alkylation of hydrocarbons catalysed by BASs of zeolites is similar to the cracking reaction. The acid sites at the intersections of ZSM-5 led to higher benzene conversion, xylene selectivity, and stability in the alkylation of benzene with methanol.[245] Moreover, previous studies indicated that the relatively "close" Al atoms providing "close" protonic sites can enhance oligomerization and hydrogen transfer reactions leading to aromatics during the catalytic cracking of 1-butene, while "single" Al atoms prefer olefin cracking.[271]

DME carbonylation to MeOAc is catalysed by the BASs of zeolite (*e.g.*, **MOR**). T_3 Al sites located in the 4MRs of the 8 and 12MR channels of **MOR** zeolite are responsible for the activity and selectivity in DME carbonylation.[297] Selectively coupled removal of T_3 and T_4 Al sites results in low activity and prolonged catalyst lifetime. Moreover, the rate of DME carbonylation exhibited a linear dependence on the amount of BASs located in the 8MR channels.[201] The Al atoms at the T_3 positions of the **MOR** 8MR channels are the active sites for DME carbonylation, which leads to the significantly prolonged catalytic lifetime and the higher selectivity of methylamine (MA), while the BASs at the 12MR channels result in coke formation and frequent deactivation.[203,297] Stronger acid sites at the 8MR channels in **MOR** zeolite could reduce the activation barriers of CO insertion to form acetyl groups, thus promoting the activity of DME carbonylation.[202]

MTO is another important BAS catalysed reaction. The catalytic performance of the RUB-13 zeolite in MTO is closely related to Al distributions and the acid density.[298] The Al atoms at the T_1 and T_2 sites are the effective acid sites that are accessible to the MTO reaction. The catalytic lifetime of H-RUB-13 increases almost linearly with an increase in the number of effective acid sites, although the selectivity to lower olefins may decrease considerably with an increase in the acid density (Fig. 13). As for ZSM-11 in the MTO reaction, increasing the proportion of Al atoms in the intersection cavity favours the aromatic cycle that preferably produces ethylene and aromatics, while the Al atoms in the straight channels favour the alkene cycle.[246] A high proportion of Al–O–Si–O–Al sequences in the framework of zeolites showed a short catalytic life in the MTO reaction compared to that with a low proportion.[273] Al atoms located across the 4MR in **CHA** zeolite generally result in weaker acids and higher activation barriers, whereas Al atoms located across the 6MR or at certain 8MR positions decrease activation barriers.[299] Therefore, the alkanol dehydration rates are enhanced on the paired Al sites located in the 6MR of **CHA**.

Selective catalytic reduction of nitrogen oxides with ammonia (NH_3-SCR) is not an acid but a Cu^{2+} catalysed reaction in which the activity and durability of the catalyst are significantly affected by the ion-exchange sites, *i.e.*, the Al location of the SSZ-13 zeolite.[266,300,301] In Cu-SSZ-13, $Cu(NH_3)_2^+$-pairs in **CHA** zeolite have been suggested to activate oxygen during low-temperature NH_3-SCR. The Al-distributions in the zeolite are found to clearly affect the probability for Cu-pair formation, which is the most favourable with an intermediate Al–Al distance of about 7.5 Å.[302] The amount of the Cu^{2+} species located in D6MRs increased linearly with the content of the paired Al species in the D6MRs of the **CHA** zeolite, which enhanced the catalytic activity for SCR of NO by NH_3.[266]

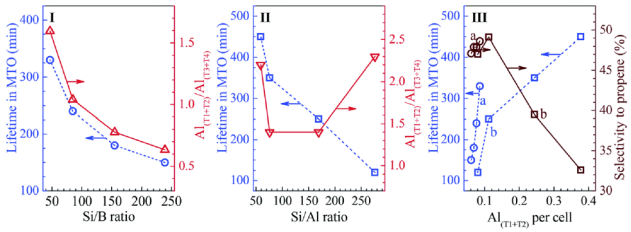

Fig. 13 (I) Effect of the Si/B ratio (Si/Al ~ 170) on the aluminium sitting in the framework and the catalytic lifetime of the H–Al–B-RUB-13-170-n series zeolites in MTO. (II) Effect of the Si/Al ratio (Si/B ≈ 17) on the aluminium sitting and the catalytic lifetime of the H–Al–B-RUB-13-m-17 series zeolites in MTO. (III) Relationship between the selectivity to propene and the catalytic lifetime of H–Al–B-RUB-13-m-n in MTO and the density of effective acid sites (represented as the number of aluminium atoms per unit cell sited at the T_1 and T_2 sites): (a) the H–Al–B-RUB-13-170-n series zeolites; (b) the H–Al–B-RUB-13-m-17 series zeolites. The MTO reactions were carried out at 400 °C with a methanol WHSV of 1.0 h^{-1}; the lifetime was determined as the reaction time when the methanol conversion decreased to 95% and the steady state selectivity to propene was reported at about 90 min on stream. Reproduced from ref. 298 with permission from the Royal Society of Chemistry, Copyright 2020.

3.4.2. Adsorption/separation. According to the equilibrium adsorption mechanism, it is expected that Al distributions will affect the adsorption energy. For example, Bulánek and co-workers investigated the influence of composition on the equilibrium CO_2 adsorption in alkali metal exchanged NaY with a Si/Al ratio of ~2.5 by combining spectroscopic, calorimetric, and theoretical studies, which yielded fine details on the CO_2 adsorption complexes and corresponding gas–solid interaction energy.[303] It was found that all CO_2 molecules are adsorbed on the cations at sites II (centre of the 6MR) of NaY *via* dispersion interactions. At a Si/Al ratio of ~2.5, the 6MR can hold only one or two Al atoms.[304] The alkali metal cation in site II containing only one Al atom has a larger partial charge than the cation in the ring having two Al atoms, which therefore has a higher polarizing capability and adsorption heat (around 2–3 kJ mol^{-1}) of CO_2 on such a site confirmed by theoretical calculations. However, this influence is relatively mild compared to that caused by the change in the Si/Al ratio of a zeolite. Lin and co-workers investigated the effects of Si/Al ratios and Al distributions of Brönsted-acid zeolites on the adsorption selectivity of *n*-alkanes *via* configurational-bias Monte Carlo simulations.[305] The adsorption selectivity in their studies is defined as the ratio of equilibrium adsorption constants for central C–C bonds relative to terminal bonds of *n*-alkanes. Their results revealed that Al distributions have a significant influence on adsorption selectivity, as much as 2-fold in the adsorption selectivity for *n*-hexane in ZSM-5. The sitting of Al atoms and their spatial proximity are two factors that substantially influence adsorption selectivity. Al atoms in close proximity have a synergistic effect on adsorbing the central C–C bonds of *n*-hexane, which results in a higher adsorption selectivity relative to isolated Al atoms. In the framework of ZSM-5, T_1, T_2, and T_{12} sites are the

three most selective T-sites for the adsorption of *n*-hexane *via* interacting with the central C–C bond of *n*-hexane, while T_4, T_5, T_6, and T_7 sites are the four least selective T-sites. These results indicate that the adsorption selectivity can be controlled by regulating the Al distributions in the framework of zeolites.

3.4.3. Ion-exchange. The influence of Al distributions on the performance of the ion-exchange of zeolites is mainly reflected in the capture of divalent ions. Al pairs provide ion-exchange sites that can capture divalent cations in zeolites because of the two close negative charges. Single Al atoms are able to accommodate exclusively monovalent cationic species, while Al pairs can stabilize divalent cations and divalent species. In addition, the Al pairs can also create two close and cooperating monovalent centers.[253] **CHA** zeolite with enriched Al pairs exhibits better adsorption performance for the divalent cation Sr^{2+}, a radioactive pollutant,[274] and Fe ions, active sites of the partial oxidation of methane.[272]

4. Summary and outlook

This review summarized the strategies and methodologies for regulating the Si/Al ratios and Al distributions of zeolites, commonly used as well as newly developed characterization techniques for determining the Si/Al ratios and Al distributions of zeolites, and their impacts on applications involving catalysis, adsorption/separation, and ion-exchange. The "bottom-up" methodologies follow the principle of regulating the Si/Al ratios of aluminosilicate oligomers. "Top-down" methodologies including steam treatment and etching with acid and/or base are the straightforward approaches to removing Al atoms or Si atoms at a specific location in the framework. Although such processes would produce a large amount of acid/base wastewater, they are suitable for large-scale industrial production. The wet chemical method (*i.e.*, ICP-AES) and XRF are the main methods for determining the Si/Al ratio in the laboratory and industry. In addition, FT-IR and XRD based methods are also developed even though their applications are limited to a specific zeolite and Si/Al ratio range. Regulating Al distributions such as sitting at a specific location and the formation of Al pairs is very challenging in the field of zeolites and is far from precise control at the present stage. Changing the Si/Al ratios and Al distributions of zeolites will undoubtedly affect their performance in catalysis, adsorption/separation, and ion-exchange. However, their correlations are far from being clarified yet.

For the synthesis of zeolites, broadening the Si/Al ratios and controlling the Al distributions are highly desired, which can tune the activity, selectivity, and durability of zeolites. Considering that zeolites are assembled by oligomers with specific Si/Al ratios and Al distributions, the efforts on regulating the Si/Al ratios and Al distributions of zeolites should focus on how to make specific oligomers with desired Si/Al ratios and Al distributions and achieve the successful assembly of such oligomers. New methodologies are desired to break the typical Si/Al limitation of zeolites and predict the Al distributions, which include high throughput techniques combined with computation predictions[306–308] and machine learning.[309] Moreover, developing new characterization techniques to unambiguously distinguish the Si and Al atoms in the framework of zeolites and the Al distributions is greatly important, which is the base to establish a clear relationship between the Al distribution and the performance of zeolites. Considering the fact that there does not exist any experimental technique to directly determine the location of aluminum or to distinguish the silicon and aluminum at framework T sites, especially within equivalent crystallographic framework T sites so far, there is an imminent and urgent need to combine theoretical calculations/simulations with *in situ*/*operando* characterization techniques at the molecular/atomic level.

In the end, the precise control of the Si/Al ratios and Al distribution of zeolites requires a molecular-level understanding of the formation mechanism of zeolites and the process of oligomer assembling, which can be achieved by combining the multi-scale simulation and the *in situ* characterization of the zeolite crystallization process.

Author contributions

Conceptualization: J. Yu and W. Yan; writing – original draft: J. Li; validation: M. Gao; writing – review & editing: J. Yu and W. Yan.

Conflicts of interest

The authors declare no conflicts of interest.

Acknowledgements

We thank the National Natural Science Foundation of China (Grants 22288101, 21920102005, U1967215, and 21835002), the National Key Research and Development Program of China (Grants 2021YFA1500401 and 2021YFA1501202), and the 111 Project (B17020) for supporting this work.

References

1 J. Smith, *Zeolites*, 1984, **4**, 309–310.
2 M. Thommes, K. Kaneko, A. V. Neimark, J. P. Olivier, F. Rodriguez-Reinoso, J. Rouquerol and K. S. W. Sing, *Pure Appl. Chem.*, 2015, **87**, 1051–1069.
3 V. Verdoliva, M. Saviano and S. De Luca, *Catalysts*, 2019, **9**, 248.
4 A. Primo and H. Garcia, *Chem. Soc. Rev.*, 2014, **43**, 7548–7561.
5 S. Standl and O. Hinrichsen, *Catalysts*, 2018, **8**, 626.
6 A. Abdelrasoul, H. Zhang, C.-H. Cheng and H. Doan, *Microporous Mesoporous Mater.*, 2017, **242**, 294–348.
7 B. Yue, S. Liu, Y. Chai, G. Wu, N. Guan and L. Li, *J. Energy Chem.*, 2022, **71**, 288–303.
8 A. Khaleque, M. M. Alam, M. Hoque, S. Mondal, J. B. Haider, B. Xu, M. A. H. Johir, A. K. Karmakar, J. L. Zhou, M. B. Ahmed and M. A. Moni, *Environ. Adv.*, 2020, **2**, 100019.
9 A. Hedström, *J. Environ. Eng.*, 2001, **127**, 673–681.

10 *Zeolite Market Size, Share & Trends Analysis Report By Application (Catalyst, Adsorbent, Detergent Builder), By Product (Natural, Synthetic), By Region (North America, Europe, APAC, CSA, MEA), And Segment Forecasts, 2022–2030*, Report 978-1-68038-601-1, Grand View Research.
11 C. Baerlocher and L. B. McCusker, *Database of Zeolite Structures*, **https://www.iza-structure.org/databases/**.
12 C. Perego, presented in part at the *Zeolite-based Catalysis, Topsøe Catalysis Forum 2005*, Havreholm Castle, Hornbæk, Denmark, August 18–19th, 2005.
13 J. Weitkamp, *Solid State Ionics*, 2000, **131**, 175–188.
14 A. Corma, *Chem. Rev.*, 1995, **95**, 559–614.
15 M. Palomino, A. Corma, F. Rey and S. Valencia, *Langmuir*, 2010, **26**, 1910–1917.
16 N. Kosinov, C. Auffret, G. J. Borghuis, V. G. P. Sripathi and E. J. M. Hensen, *J. Membr. Sci.*, 2015, **484**, 140–145.
17 M. Fasano, T. Humplik, A. Bevilacqua, M. Tsapatsis, E. Chiavazzo, E. N. Wang and P. Asinari, *Nat. Commun.*, 2016, **7**, 12762.
18 A. Osatiashtiani, B. Puértolas, C. C. S. Oliveira, J. C. Manayil, B. Barbero, M. Isaacs, C. Michailof, E. Heracleous, J. Pérez-Ramírez, A. F. Lee and K. Wilson, *Biomass Convers. Biorefin.*, 2017, **7**, 331–342.
19 C. Wang, S. Leng, H. Guo, J. Yu, W. Li, L. Cao and J. Huang, *Appl. Surf. Sci.*, 2019, **498**, 143874.
20 C. J. Heard, L. Grajciar, F. Uhlik, M. Shamzhy, M. Opanasenko, J. Cejka and P. Nachtigall, *Adv. Mater.*, 2020, **32**, 2003264.
21 G. Agostini, C. Lamberti, L. Palin, M. Milanesio, N. Danilina, B. Xu, M. Janousch and J. A. Van Bokhoven, *J. Am. Chem. Soc.*, 2010, **132**, 667–678.
22 M. D. Oleksiak, K. Muraoka, M. F. Hsieh, M. T. Conato, A. Shimojima, T. Okubo, W. Chaikittisilp and J. D. Rimer, *Angew. Chem., Int. Ed.*, 2017, **56**, 13366–13371.
23 D. Zhu, L. Wang, D. Fan, N. Yan, S. Huang, S. Xu, P. Guo, M. Yang, J. Zhang, P. Tian and Z. Liu, *Adv. Mater.*, 2020, **32**, 2000272.
24 D. Zhu, L. Wang, W. Zhang, D. Fan, J. Li, W. Cui, S. Huang, S. Xu, P. Tian and Z. Liu, *Angew. Chem., Int. Ed.*, 2022, **61**, e202117698.
25 C. W. McDaniel and P. K. Maher, in *Molecular Sieves*, Society of Chemical Industry, London, UK, 1968, p. 186.
26 N. Cui, H. Guo, J. Zhou, L. Li, L. Guo and Z. Hua, *Microporous Mesoporous Mater.*, 2020, **306**, 110411.
27 S. Kim, G. Park, M. H. Woo, G. Kwak and S. K. Kim, *ACS Catal.*, 2019, **9**, 2880–2892.
28 Y. Xue, J. Li, P. Wang, X. Cui, H. Zheng, Y. Niu, M. Dong, Z. Qin, J. Wang and W. Fan, *Appl. Catal., B*, 2021, **280**, 119391.
29 T. Liang, J. Chen, Z. Qin, J. Li, P. Wang, S. Wang, G. Wang, M. Dong, W. Fan and J. Wang, *ACS Catal.*, 2016, **6**, 7311–7325.
30 Q. Ke, I. Khalil, B. Smeyers, Z. Li, R. de Oliveira-Silva, B. Sels, D. Sakellariou and M. Dusselier, *Angew. Chem., Int. Ed.*, 2021, **60**, 24189–24197.
31 E. Salvadori, E. Fusco and M. Chiesa, *J. Phys. Chem. Lett.*, 2022, **13**, 1283–1289.
32 Z. Mi, T. Lu, J.-N. Zhang, R. Xu and W. Yan, *Chem. Res. Chin. Univ.*, 2021, **38**, 9–17.
33 S. J. Kwak, H. S. Kim, N. Park, M.-J. Park and W. B. Lee, *Korean J. Chem. Eng.*, 2021, **38**, 1117–1128.
34 A. Palčić and V. Valtchev, *Appl. Catal., A*, 2020, **606**, 117795.
35 J. Dědeček, Z. Sobalík and B. Wichterlová, *Catal. Rev.: Sci. Eng.*, 2012, **54**, 135–223.
36 M. Ciantar, T. T. Trinh, C. Michel, P. Sautet, C. Mellot-Draznieks and C. Nieto-Draghi, *Angew. Chem., Int. Ed.*, 2021, **60**, 7111–7116.
37 C. Lei, Z. Dong, C. Martinez, J. Martinez-Triguero, W. Chen, Q. Wu, X. Meng, A. N. Parvulescu, T. De Baerdemaeker, U. Muller, A. Zheng, Y. Ma, W. Zhang, T. Yokoi, B. Marler, D. E. De Vos, U. Kolb, A. Corma and F. S. Xiao, *Angew. Chem., Int. Ed.*, 2020, **59**, 15649–15655.
38 K. Asselman, N. Pellens, B. Thijs, N. Doppelhammer, M. Haouas, F. Taulelle, J. A. Martens, E. Breynaert and C. E. A. Kirschhock, *Chem. Mater.*, 2022, **34**, 7150–7158.
39 R. Otomo and T. Yokoi, *Microporous Mesoporous Mater.*, 2016, **224**, 155–162.
40 P. Sazama, B. Wichterlová, Š. Sklenák, V. I. Parvulescu, N. Candu, G. Sádovská, J. Dědeček, P. Klein, V. Pashkova and P. Šťastný, *J. Catal.*, 2014, **318**, 22–33.
41 B. Yilmaz, U. Müller, M. Feyen, S. Maurer, H. Zhang, X. Meng, F.-S. Xiao, X. Bao, W. Zhang and H. Imai, *Catal. Sci. Technol.*, 2013, **3**, 2580–2586.
42 R. Pilar, J. Moravkova, G. Sadovska, S. Sklenak, L. Brabec, J. Pastvova and P. Sazama, *Microporous Mesoporous Mater.*, 2022, **333**, 111726.
43 P. Luo, H. Xu, T. Xue, J. Jiang, H. Wu, M. He and P. Wu, *Inorg. Chem. Front.*, 2021, **8**, 1574–1587.
44 B. Meng, S. Ren, Z. Li, S. Nie, X. Zhang, W. Song, Q. Guo and B. Shen, *Microporous Mesoporous Mater.*, 2021, **323**, 111248.
45 L. Han, R. Wang, P. Wang, A. Zheng, Y. Guo, Y. Chen, Q. Jiang and W. Lin, *Catal. Sci. Technol.*, 2021, **11**, 6089–6095.
46 I. A. Bakare, O. Muraza, M. A. Sanhoob, K. Miyake, Y. Hirota, Z. H. Yamani and N. Nishiyama, *Fuel*, 2018, **211**, 18–26.
47 H. Zhang, C. Wu, M. Song, T. Lu, W. Wang, Z. Wang, W. Yan, P. Cheng and Z. Zhao, *Microporous Mesoporous Mater.*, 2021, **310**, 110633.
48 W. Löwenstein, *Am. Mineral.*, 1954, **39**, 92–96.
49 B. Wang, L. Ren, J. Zhang, R. Peng, S. Jin, Y. Guan, H. Xu and P. Wu, *Microporous Mesoporous Mater.*, 2021, **314**, 110894.
50 J. Wang, P. Liu, M. Boronat, P. Ferri, Z. Xu, P. Liu, B. Shen, Z. Wang and J. Yu, *Angew. Chem., Int. Ed.*, 2020, **59**, 17225–17228.
51 T. Fu, J. Shao and Z. Li, *Appl. Catal., B*, 2021, **291**, 120098.
52 C. Jonscher, M. Seifert, N. Kretzschmar, M. S. Marschall, M. Le Anh, T. Doert, O. Busse and J. J. Weigand, *ChemCatChem*, 2022, **14**, e202101248.
53 C. S. Cundy and P. A. Cox, *Microporous Mesoporous Mater.*, 2005, **82**, 1–78.

54 S. Mintova, V. Valtchev, T. Onfroy, C. Marichal, H. Knözinger and T. Bein, *Microporous Mesoporous Mater.*, 2006, **90**, 237–245.
55 G. Majano, L. Delmotte, V. Valtchev and S. Mintova, *Chem. Mater.*, 2009, **21**, 4184–4191.
56 B. Zheng, Y. Wan, W. Yang, F. Ling, H. Xie, X. Fang and H. Guo, *Chin. J. Catal.*, 2014, **35**, 1800–1810.
57 K. Itabashi, Y. Kamimura, K. Iyoki, A. Shimojima and T. Okubo, *J. Am. Chem. Soc.*, 2012, **134**, 11542–11549.
58 A. Vallace, G. C. Kester, C. Bongo, W. Casteel, G. Lau, R. Whitley and C. G. Coe, *Microporous Mesoporous Mater.*, 2021, **312**, 110755.
59 Y. Kamimura, S. Tanahashi, K. Itabashi, A. Sugawara, T. Wakihara, A. Shimojima and T. Okubo, *J. Phys. Chem. C*, 2011, **115**, 744–750.
60 L. Wang, P. Tian, Y. Yuan, M. Yang, D. Fan, H. Zhou, W. Zhu, S. Xu and Z. Liu, *Microporous Mesoporous Mater.*, 2014, **196**, 89–96.
61 D. Zhu, L. Wang, W. Cui, J. Tan, P. Tian and Z. Liu, *Inorg. Chem. Front.*, 2022, **9**, 2213–2220.
62 H. Luan, C. Lei, Y. Ma, Q. Wu, L. Zhu, H. Xu, S. Han, Q. Zhu, X. Liu, X. Meng and F.-S. Xiao, *Chin. J. Catal.*, 2021, **42**, 563–570.
63 Q. Wu, L. Zhu, Y. Chu, X. Liu, C. Zhang, J. Zhang, H. Xu, J. Xu, F. Deng, Z. Feng, X. Meng and F. S. Xiao, *Angew. Chem., Int. Ed.*, 2019, **58**, 12138–12142.
64 S. Goel, S. I. Zones and E. Iglesia, *Chem. Mater.*, 2015, **27**, 2056–2066.
65 L. Tang, K.-G. Haw, Y. Zhang, Q. Fang, S. Qiu and V. Valtchev, *Microporous Mesoporous Mater.*, 2019, **280**, 306–314.
66 M. Itakura, Y. Oumi, M. Sadakane and T. Sano, *Mater. Res. Bull.*, 2010, **45**, 646–650.
67 M. Itakura, I. Goto, A. Takahashi, T. Fujitani, Y. Ide, M. Sadakane and T. Sano, *Microporous Mesoporous Mater.*, 2011, **144**, 91–96.
68 X. Xiong, D. Yuan, Q. Wu, F. Chen, X. Meng, R. Lv, D. Dai, S. Maurer, R. McGuire, M. Feyen, U. Müller, W. Zhang, T. Yokoi, X. Bao, H. Gies, B. Marler, D. E. De Vos, U. Kolb, A. Moini and F.-S. Xiao, *J. Mater. Chem. A*, 2017, **5**, 9076–9080.
69 Y. Li, K. Zhang, Y. Chen, Y. Zhang, X. Liang, L. Han, X. Li and P. Han, *J. Solid State Chem.*, 2021, **293**, 121769.
70 A. Vallace, G. Kester, W. Casteel, G. Lau, R. Whitley and C. Coe, *J. Phys. Chem. C*, 2021, **125**, 12848–12856.
71 H. Jon, K. Nakahata, B. Lu, Y. Oumi and T. Sano, *Microporous Mesoporous Mater.*, 2006, **96**, 72–78.
72 C. Sun, W. Chen, J. Wang, S. Wang, Z. Ma, M. Chen, A. Zheng, W. Yan and J. Yu, *Inorg. Chem. Front.*, 2022, **9**, 1293–1299.
73 C. Sun, Z. Liu, S. Wang, H. Pang, R. Bai, Q. Wang, W. Chen, A. Zheng, W. Yan and J. Yu, *CCS Chem.*, 2021, **3**, 189–198.
74 G. Feng, P. Cheng, W. Yan, M. Boronat, X. Li, J.-H. Su, J. Wang, Y. Li, A. Corma and R. Xu, *Science*, 2016, **351**, 1188–1191.
75 Q. Zhang, S. Xiang, Q. Zhang, B. Wang, A. Mayoral, W. Liu, Y. Wang, Y. Liu, J. Shi, G. Yang, J. Luo, X. Chen, O. Terasaki, J.-P. Gilson and J. Yu, *Chem. Mater.*, 2019, **32**, 751–758.
76 S. Mintova, J. P. Gilson and V. Valtchev, *Nanoscale*, 2013, **5**, 6693–6703.
77 J. Li, M. Liu, X. Guo, C. Dai and C. Song, *J. Energy Chem.*, 2018, **27**, 1225–1230.
78 Z. Qin, L. Lakiss, L. Tosheva, J.-P. Gilson, A. Vicente, C. Fernandez and V. Valtchev, *Adv. Funct. Mater.*, 2014, **24**, 257–264.
79 X. Zhao, L. Wang, J. Li, S. Xu, W. Zhang, Y. Wei, X. Guo, P. Tian and Z. Liu, *Catal. Sci. Technol.*, 2017, **7**, 5882–5892.
80 X. Zhao, L. Wang, P. Guo, N. Yan, T. Sun, S. Lin, X. Guo, P. Tian and Z. Liu, *Catal. Sci. Technol.*, 2018, **8**, 2966–2974.
81 H. Kacirek and H. Lechert, *J. Phys. Chem.*, 1976, **80**, 1291–1296.
82 F. Delprato, L. Delmotte, J. Guth and L. Huve, *Zeolites*, 1990, **10**, 546–552.
83 L. Zhu, L. Ren, S. Zeng, C. Yang, H. Zhang, X. Meng, M. Rigutto, A. Made and F. S. Xiao, *Chem. Commun.*, 2013, **49**, 10495–10497.
84 D. Yuan, D. He, S. Xu, Z. Song, M. Zhang, Y. Wei, Y. He, S. Xu, Z. Liu and Y. Xu, *Microporous Mesoporous Mater.*, 2015, **204**, 1–7.
85 D. He, D. Yuan, Z. Song, Y. Tong, Y. Wu, S. Xu, Y. Xu and Z. Liu, *Chem. Commun.*, 2016, **52**, 12765–12768.
86 D. He, D. Yuan, Z. Song, Y. Xu and Z. Liu, *Chin. J. Catal.*, 2019, **40**, 52–59.
87 O. Larlus, S. Mintova, S. T. Wilson, R. R. Willis, H. Abrevaya and T. Bein, *Microporous Mesoporous Mater.*, 2011, **142**, 17–25.
88 R. Martinez-Franco, C. Paris, M. E. Martinez-Armero, C. Martinez, M. Moliner and A. Corma, *Chem. Sci.*, 2016, **7**, 102–108.
89 F. Collins, A. Rozhkovskaya, J. G. Outram and G. J. Millar, *Microporous Mesoporous Mater.*, 2020, **291**, 109667.
90 M. B. Park, Y. Lee, A. Zheng, F. S. Xiao, C. P. Nicholas, G. J. Lewis and S. B. Hong, *J. Am. Chem. Soc.*, 2013, **135**, 2248–2255.
91 A. Corma, F. Rey, J. Rius, M. J. Sabater and S. Valencia, *Nature*, 2004, **431**, 287–290.
92 B. W. Boal, J. E. Schmidt, M. A. Deimund, M. W. Deem, L. M. Henling, S. K. Brand, S. I. Zones and M. E. Davis, *Chem. Mater.*, 2015, **27**, 7774–7779.
93 D. Jo, G. T. Park, T. Ryu and S. B. Hong, *Appl. Catal., B*, 2019, **243**, 212–219.
94 D. Jo, T. Ryu, G. T. Park, P. S. Kim, C. H. Kim, I.-S. Nam and S. B. Hong, *ACS Catal.*, 2016, **6**, 2443–2447.
95 W. Xu, J. Dong, J. Li, J. Li and F. Wu, *J. Chem. Soc., Chem. Commun.*, 1990, 755–756.
96 Y. Shinno, K. Iyoki, K. Ohara, Y. Yanaba, Y. Naraki, T. Okubo and T. Wakihara, *Angew. Chem., Int. Ed.*, 2020, **59**, 20099–20103.
97 H. Al Jabri, K. Miyake, K. Ono, M. Nakai, Y. Hirota, Y. Uchida, M. Miyamoto and N. Nishiyama, *Microporous Mesoporous Mater.*, 2019, **278**, 322–326.

98 V. Vattipalli, A. M. Paracha, W. Hu, H. Chen and W. Fan, *Angew. Chem., Int. Ed.*, 2018, **57**, 3607–3611.
99 Y. Luo, M. Li, X. Lv, Q. Huang and X. Chen, *Microporous Mesoporous Mater.*, 2020, **293**, 109675.
100 J. V. Milato, R. J. França, A. S. Rocha and M. R. C. M. Calderari, *J. Anal. Appl. Pyrolysis*, 2020, **151**, 104928.
101 C. Pagis, A. R. Morgado Prates, N. Bats, A. Tuel and D. Farrusseng, *CrystEngComm*, 2018, **20**, 1564–1572.
102 V. Babić, L. Tang, Z. Qin, L. Hafiz, J. P. Gilson and V. Valtchev, *Adv. Mater. Interfaces*, 2020, **8**, 2000348.
103 R. Zhang, R. Zou, W. Li, Y. Chang and X. Fan, *Microporous Mesoporous Mater.*, 2022, **333**, 111736.
104 C. Chen, Z. Hu, J. Ren, S. Zhang, Z. Wang and Z.-Y. Yuan, *ChemCatChem*, 2019, **11**, 868–877.
105 R. Otomo, U. Müller, M. Feyen, B. Yilmaz, X. Meng, F.-S. Xiao, H. Gies, X. Bao, W. Zhang, D. De Vos and T. Yokoi, *Catal. Sci. Technol.*, 2016, **6**, 713–721.
106 F. Yi, Y. Chen, Z. Tao, C. Hu, X. Yi, A. Zheng, X. Wen, Y. Yun, Y. Yang and Y. Li, *J. Catal.*, 2019, **380**, 204–214.
107 X. Guo, L. Guo, Y. Zeng, R. Kosol, X. Gao, Y. Yoneyama, G. Yang and N. Tsubaki, *Catal. Today*, 2021, **368**, 196–203.
108 F. Yi, H. Chen, L. Huang, C. Hu, J. Wang, T. Li, H. Wang, Z. Tao, Y. Yang and Y. Li, *Fuel*, 2021, **300**, 120694.
109 R. Giudici, H. Kouwenhoven and R. Prins, *Appl. Catal., A*, 2000, **203**, 101–110.
110 A. Maghfirah, Y. Susanti, A. T. N. Fajar, R. R. Mukti and G. T. M. Kadja, *Mater. Res. Express*, 2019, **6**, 094002.
111 D. V. Peron, V. L. Zholobenko, J. H. S. de Melo, M. Capron, N. Nuns, M. O. de Souza, L. A. Feris, N. R. Marcilio, V. V. Ordomsky and A. Y. Khodakov, *Microporous Mesoporous Mater.*, 2019, **286**, 57–64.
112 X. Zhang, M. Yang, P. Tian and Z. Liu, *Chem. Res. Chin. Univ.*, 2022, 1–8.
113 O. Pliekhov, O. Pliekhova, I. Arčon, F. Bondino, E. Magnano, G. Mali and N. Z. Logar, *Microporous Mesoporous Mater.*, 2020, **302**, 110208.
114 V. Babić, S. Koneti, S. Moldovan, M. Debost, J.-P. Gilson and V. Valtchev, *Microporous Mesoporous Mater.*, 2022, **329**, 111513.
115 S. Abdulridha, Y. Jiao, S. Xu, R. Zhang, A. A. Garforth and X. Fan, *Front. Chem.*, 2020, **8**, 482.
116 R. Zhang, D. Raja, Y. Zhang, Y. Yan, A. A. Garforth, Y. Jiao and X. Fan, *Top. Catal.*, 2020, **63**, 340–350.
117 Y. Liu, D. Zheng, B. Li, Y. Lyu, X. Wang, X. Liu, L. Li, S. Yu, X. Liu and Z. Yan, *Microporous Mesoporous Mater.*, 2020, **299**, 110117.
118 A. Bolshakov, N. Kosinov, D. E. Romero Hidalgo, B. Mezari, A. J. F. van Hoof and E. J. M. Hensen, *Catal. Sci. Technol.*, 2019, **9**, 4239–4247.
119 A. Feng, Y. Yu, L. Mi, Y. Cao, Y. Yu and L. Song, *Microporous Mesoporous Mater.*, 2019, **280**, 211–218.
120 X. Zhu, N. Kosinov, A. V. Kubarev, A. Bolshakov, B. Mezari, I. Valastyan, J. P. Hofmann, M. B. J. Roeffaers, E. Sarkadi-Pribóczki and E. J. M. Hensen, *ChemCatChem*, 2017, **9**, 3470–3477.
121 M. Li, Y. Zhou, C. Ju and Y. Fang, *Appl. Catal., A*, 2016, **512**, 1–8.
122 X. Chen, A. Vicente, Z. Qin, V. Ruaux, J. P. Gilson and V. Valtchev, *Chem. Commun.*, 2016, **52**, 3512–3515.
123 H. Beyer, G. Borbély-Pálné and J. Wu, in *Stud. Surf. Sci. Catal.*, Elsevier, 1994, vol. 84, pp. 933–940.
124 J. M. Müller, G. C. Mesquita, S. M. Franco, L. D. Borges, J. L. de Macedo, J. A. Dias and S. C. L. Dias, *Microporous Mesoporous Mater.*, 2015, **204**, 50–57.
125 L. D. Borges and J. L. de Macedo, *Microporous Mesoporous Mater.*, 2016, **236**, 85–93.
126 Y. Wang, T. Yokoi, S. Namba, J. N. Kondo and T. Tatsumi, *Appl. Catal., A*, 2015, **504**, 192–202.
127 G. Pál-Borbély and H. K. Beyer, *Phys. Chem. Chem. Phys.*, 2003, **5**, 2145–2153.
128 Y. Wang, R. Otomo, T. Tatsumi and T. Yokoi, *Microporous Mesoporous Mater.*, 2016, **220**, 275–281.
129 Y. Zhang, H. Wang and R. Chen, *RSC Adv.*, 2015, **5**, 67841–67848.
130 M. W. Anderson and J. Klinowski, *J. Chem. Soc., Faraday Trans.*, 1986, **82**, 1449–1469.
131 H. K. Beyer, I. M. Belenykaja, F. Hange, M. Tielen, P. J. Grobet and P. A. Jacobs, *J. Chem. Soc., Faraday Trans.*, 1985, **81**, 2889–2901.
132 B. Sulikowski, G. Borbely, H. Beyer, H. G. Karge and I. Mishin, *J. Phys. Chem.*, 1989, **93**, 3240–3243.
133 H. K. Beyer and I. Belenykaja, in *Stud. Surf. Sci. Catal.*, Elsevier, 1980, vol. 5, pp. 203–210.
134 L. Kubelková, V. Seidl, J. Nováková, S. Bednářová and P. Jírů, *J. Chem. Soc., Faraday Trans.*, 1984, **80**, 1367–1376.
135 J. Klinowski, J. Thomas, C. Fyfe, G. Gobbi and J. Hartman, *Inorg. Chem.*, 1983, **22**, 63–66.
136 Z. Shi, P. Ji, Z. Zhu, J.-g. Jiang, W. Fu, P. Wu, Y. Wang and M. He, *ChemCatChem*, 2016, **8**, 1891–1895.
137 B. Fan, D. Zhu, L. Wang, S. Xu, Y. Wei and Z. Liu, *Inorg. Chem. Front.*, 2022, **9**, 3609–3618.
138 G. T. Kerr, *J. Phys. Chem.*, 1967, **71**, 4155–4156.
139 G. Hutchings and C. Kiely, *J. Chem. Soc., Faraday Trans.*, 1997, **93**, 3593–3598.
140 S. Morin, A. Berreghis, P. Ayrault, N. Gnep and M. Guisnet, *J. Chem. Soc., Faraday Trans.*, 1997, **93**, 3269–3275.
141 F. Xu, J. Lv, C. Chen, Z. Hong, G. Zhao, L. Miao, W. Yang and Z. Zhu, *Ind. Eng. Chem. Res.*, 2022, **61**, 1258–1266.
142 Z. Huang, J. Zhang, Q. Han, X. Zhang, P. Lu, L. Xu, Y. Yuan and L. Xu, *Appl. Catal., A*, 2019, **572**, 80–89.
143 B. J. B. Silva, L. V. Sousa, L. R. A. Sarmento, R. P. Carvalho, P. H. L. Quintela, J. G. A. Pacheco, R. Fréty and A. O. S. Silva, *Microporous Mesoporous Mater.*, 2019, **290**, 109647.
144 S. Yang, C. Yu, L. Yu, S. Miao, M. Zou, C. Jin, D. Zhang, L. Xu and S. Huang, *Angew. Chem., Int. Ed.*, 2017, **56**, 12553–12556.
145 C. Pagis, A. Guesdon Vennerie, A. R. Morgado Prates, N. Bats, A. Tuel and D. Farrusseng, *Microporous Mesoporous Mater.*, 2018, **265**, 123–131.
146 G. Xu, P. Zhang, J. Cheng, T. Wei, X. Zhu and F. Yang, *J. Solid State Chem.*, 2021, **300**, 122238.

147 S. Fernandez, M. L. Ostraat, J. A. Lawrence and K. Zhang, *Microporous Mesoporous Mater.*, 2018, **263**, 201–209.
148 T. Li, J. Ihli, Z. Ma, F. Krumeich and J. A. van Bokhoven, *J. Phys. Chem. C*, 2019, **123**, 8793–8801.
149 A. R. Morgado Prates, T. Chetot, L. Burel, C. Pagis, R. Martinez-Franco, M. Dodin, D. Farrusseng and A. Tuel, *J. Solid State Chem.*, 2020, **281**, 121033.
150 D. Verboekend, S. Mitchell, M. Milina, J. C. Groen and J. Pérez-Ramírez, *J. Phys. Chem. C*, 2011, **115**, 14193–14203.
151 J. Ding, M. Wang, L. Peng, N. Xue, Y. Wang and M.-Y. He, *Appl. Catal., A*, 2015, **503**, 147–155.
152 E. Catizzone, M. Migliori, A. Aloise, R. Lamberti and G. Giordano, *J. Mater. Chem.*, 2019, **2019**, 1–9.
153 T. C. Hoff, D. W. Gardner, R. Thilakaratne, J. Proano-Aviles, R. C. Brown and J.-P. Tessonnier, *Appl. Catal., A*, 2017, **529**, 68–78.
154 K. Pyra, K. A. Tarach, D. Majda and K. Góra-Marek, *Catal. Sci. Technol.*, 2019, **9**, 1794–1801.
155 K. A. Tarach, J. Martinez-Triguero, F. Rey and K. Góra-Marek, *J. Catal.*, 2016, **339**, 256–269.
156 S. Akyalcin, L. Akyalcin and M. Bjørgen, *Microporous Mesoporous Mater.*, 2019, **273**, 256–264.
157 Y.-K. Ma, S. Rigolet, L. Michelin, J.-L. Paillaud, S. Mintova, F. Khoerunnisa, T. J. Daou and E.-P. Ng, *Microporous Mesoporous Mater.*, 2021, **311**, 110683.
158 D. E. Newbury and N. W. Ritchie, *Scanning*, 2013, **35**, 141–168.
159 J. R. Shallenberger, N. J. Smith and J. Banerjee, *Surf. Interface Anal.*, 2021, **53**, 569–579.
160 B. Beckhoff, B. Kanngießer, N. Langhoff, R. Wedell and H. Wolff, *Handbook of Practical X-ray Fluorescence Analysis*, Springer Science & Business Media, 2007.
161 E. Urquieta-González, L. Martins, R. Peguin and M. Batista, *Mater. Res.*, 2002, **5**, 321–327.
162 B. Xu, S. Bordiga, R. Prins and J. A. van Bokhoven, *Appl. Catal., A*, 2007, **333**, 245–253.
163 J. R. Di Iorio and R. Gounder, *Chem. Mater.*, 2016, **28**, 2236–2247.
164 P. A. S. Moura, E. Rodríguez-Aguado, D. A. S. Maia, D. C. Melo, R. Singh, S. Valencia, P. A. Webley, F. Rey, M. Bastos-Neto, E. Rodríguez-Castellón and D. C. S. Azevedo, *Catal. Today*, 2022, **390–391**, 99–108.
165 R. Hajjar, Y. Millot, P. P. Man, M. Che and S. Dzwigaj, *J. Phys. Chem. C*, 2008, **112**, 20167–20175.
166 J. Klinowski, *Annu. Rev. Mater. Sci.*, 1988, **18**, 189–218.
167 C. Fyfe, G. Gobbi, G. Kennedy, J. Graham, R. Ozubko, W. Murphy, A. Bothner-By, J. Dadok and A. Chesnick, *Zeolites*, 1985, **5**, 179–183.
168 R. Jarman, A. Jacobson and M. Melchior, *J. Phys. Chem.*, 1984, **88**, 5748–5752.
169 M. Sadrara, M. Khanmohammadi Khorrami, J. Towfighi Darian and A. Bagheri Garmarudi, *Infrared Phys. Technol.*, 2021, **116**, 103797.
170 U. Lohse, I. Pitsch, E. Schreier, B. Parlitz and K.-H. Schnabel, *Appl. Catal., A*, 1995, **129**, 189–202.
171 T. Armaroli, L. J. Simon, M. Digne, T. Montanari, M. Bevilacqua, V. Valtchev, J. Patarin and G. Busca, *Appl. Catal., A*, 2006, **306**, 78–84.
172 H. Fichtner-Schmittler, U. Lohse, H. Miessner and H.-E. Maneck, *Z. Phys. Chem.*, 1990, **271**, 69–80.
173 T. T. Le, K. Shilpa, C. Lee, S. Han, C. Weiland, S. R. Bare, P. J. Dauenhauer and J. D. Rimer, *J. Catal.*, 2022, **405**, 664–675.
174 Y. Wang, X. Liu, W. Zhang, Z. Li, Y. Zhang, Y. Li and Y. Ren, *J. Cleaner Prod.*, 2020, **244**, 118852.
175 L. Yu, S. Fouladvand, M. Grahn and J. Hedlund, *Microporous Mesoporous Mater.*, 2019, **284**, 258–264.
176 T. F. Chaves, H. O. Pastore, P. Hammer and D. Cardoso, *Microporous Mesoporous Mater.*, 2015, **202**, 198–207.
177 M. Khosravi, H. E. Cathey and I. D. R. Mackinnon, *Microporous Mesoporous Mater.*, 2021, **312**, 110753.
178 P. S. Neuhoff and L. S. Ruhl, *Chem. Geol.*, 2006, **225**, 373–387.
179 J. F. Haw, *Phys. Chem. Chem. Phys.*, 2002, **4**, 5431–5441.
180 D. J. Mihalcik, C. A. Mullen and A. A. Boateng, *J. Anal. Appl. Pyrolysis*, 2011, **92**, 224–232.
181 R. Hansford, *Ind. Eng. Chem.*, 1947, **39**, 849–852.
182 V. Doronin and T. Sorokina, *Russ. J. Gen. Chem.*, 2007, **77**, 2224–2231.
183 T. Chen, C. Gu, Y. Ouyang, L. Zhuang, Z. Yao, K. Zou, Y. Wang, Y. Luo and X. Shu, *Fuel*, 2022, **318**, 123696.
184 W. Wang, W. Zhang, Y. Chen, X. Wen, H. Li, D. Yuan, Q. Guo, S. Ren, X. Pang and B. Shen, *J. Catal.*, 2018, **362**, 94–105.
185 K. Khivantsev, N. R. Jaegers, L. Kovarik, M. A. Derewinski, J. H. Kwak and J. Szanyi, *Molecules*, 2022, **27**, 2352.
186 K. Tarach, K. Góra-Marek, J. Tekla, K. Brylewska, J. Datka, K. Mlekodaj, W. Makowski, M. C. Igualada López, J. Martínez Triguero and F. Rey, *J. Catal.*, 2014, **312**, 46–57.
187 Y. Wang, J. Li, W. Tong, Z. Shen, L. Li, Q. Zhang and J. Yu, *Inorg. Chem. Front.*, 2022, **9**, 2470–2478.
188 J. Meng, C. Li, X. Chen, C. Song and C. Liang, *Microporous Mesoporous Mater.*, 2020, **309**, 110565.
189 M. Rahman, A. Infantes-Molina, A. S. Hoffman, S. R. Bare, K. L. Emerson and S. J. Khatib, *Fuel*, 2020, **278**, 118290.
190 Z. Yang, R. Zhang, F. Dai, H. Tang, R. Liu and S. Zhang, *Energy Fuels*, 2020, **34**, 9426–9435.
191 A. Fink, C. H. Gierlich, I. Delidovich and R. Palkovits, *ChemCatChem*, 2020, **12**, 5710–5719.
192 Y. Zhang, W. Dai, G. Wu, N. Guan and L. Li, *Chem. Res. Chin. Univ.*, 2021, **38**, 173–180.
193 D. Stepanenko and Z. Kneba, *Combust. Engines*, 2019, **177**, 172–179.
194 P. Haro, F. Trippe, R. Stahl and E. Henrich, *Appl. Energy*, 2013, **108**, 54–65.
195 W. Alharbi, E. F. Kozhevnikova and I. V. Kozhevnikov, *ACS Catal.*, 2015, **5**, 7186–7193.
196 M. Marosz, B. Samojeden, A. Kowalczyk, M. Rutkowska, M. Motak, U. Diaz, A. E. Palomares and L. Chmielarz, *Materials*, 2020, **13**, 2399.
197 X. Sun, Y. Yang, Y. He, S. Zhu and Z. Liu, *Catal. Lett.*, 2020, **151**, 2004–2010.

198 Y. Liu, K. Murata, M. Inaba and I. Takahara, *Fuel Process. Technol.*, 2013, **110**, 206–213.
199 P. Cheung, A. Bhan, G. Sunley, D. Law and E. Iglesia, *J. Catal.*, 2007, **245**, 110–123.
200 M. Boronat, C. Martínez-Sánchez, D. Law and A. Corma, *J. Am. Chem. Soc.*, 2008, **130**, 16316–16323.
201 M. Wang, S. Huang, J. Lü, Z. Cheng, Y. Li, S. Wang and X. Ma, *Chin. J. Catal.*, 2016, **37**, 1530–1537.
202 K. Cai, S. Huang, Y. Li, Z. Cheng, J. Lv and X. Ma, *ACS Sustainable Chem. Eng.*, 2018, **7**, 2027–2034.
203 R. Liu, B. Fan, W. Zhang, L. Wang, L. Qi, Y. Wang, S. Xu, Z. Yu, Y. Wei and Z. Liu, *Angew. Chem., Int. Ed.*, 2022, **61**, e202116990.
204 M. Yang, D. Fan, Y. Wei, P. Tian and Z. Liu, *Adv. Mater.*, 2019, **31**, 1902181.
205 S. Svelle, F. Joensen, J. Nerlov, U. Olsbye, K.-P. Lillerud, S. Kolboe and M. Bjørgen, *J. Am. Chem. Soc.*, 2006, **128**, 14770–14771.
206 M. Bjørgen, F. Joensen, K.-P. Lillerud, U. Olsbye and S. Svelle, *Catal. Today*, 2009, **142**, 90–97.
207 M. Guisnet, L. Costa and F. R. Ribeiro, *J. Mol. Catal. A: Chem.*, 2009, **305**, 69–83.
208 U. Olsbye, S. Svelle, M. Bjorgen, P. Beato, T. V. Janssens, F. Joensen, S. Bordiga and K. P. Lillerud, *Angew. Chem., Int. Ed.*, 2012, **51**, 5810–5831.
209 S. Wang, P. Wang, Z. Qin, Y. Chen, M. Dong, J. Li, K. Zhang, P. Liu, J. Wang and W. Fan, *ACS Catal.*, 2018, **8**, 5485–5505.
210 M. Dusselier, P. Van Wouwe, A. Dewaele, P. A. Jacobs and B. F. Sels, *Science*, 2015, **349**, 78–80.
211 Z. Ma, Q. Zhang, L. Li, M. Chen, J. Li and J. Yu, *Chem. Sci.*, 2022, **13**, 8052–8059.
212 A. Corma and A. Martinez, *Adv. Mater.*, 1995, **7**, 137–144.
213 J. Pérez-Pellitero and G. D. Pirngruber, in *New Developments in Adsorption/Separation of Small Molecules by Zeolites*, Springer, 2020, pp. 195–225.
214 R. T. Yang, *Adsorbents: fundamentals and applications*, John Wiley & Sons, 2003.
215 C. C. Chao, *US Pat.*, 4859217, Assignee: UOP, 1989.
216 F. E. Epiepang, X. Yang, J. Li, Y. Liu and R. T. Yang, *AIChEJ.*, 2018, **64**, 406–415.
217 X. Yang, F. E. Epiepang, J. Li, Y. Wei, Y. Liu and R. T. Yang, *Chem. Eng. J.*, 2019, **362**, 482–486.
218 S. J. Weigel, J. E. Macdougall, C. G. Coe, Y. L. Xiong, J. A. Martens, P. A. Jacobs and P. A. Webley, *US Pat.*, 5779766, Assignee: Air Products and Chemicals, Inc., 1998.
219 Y. Wang, Q. Zhang and J. Yu, *Chem. J. Chin. Univ.*, 2020, **41**, 616–622.
220 S. Wang, P. Bai, M. Sun, W. Liu, D. Li, W. Wu, W. Yan, J. Shang and J. Yu, *Adv. Sci.*, 2019, **6**, 1901317.
221 M. Sai Bhargava Reddy, D. Ponnamma, K. K. Sadasivuni, B. Kumar and A. M. Abdullah, *RSC Adv.*, 2021, **11**, 12658–12681.
222 T. S. Frantz, W. A. Ruiz, C. A. da Rosa and V. B. Mortola, *Microporous Mesoporous Mater.*, 2016, **222**, 209–217.
223 Y. Guo, T. Sun, Y. Gu, X. Liu, Q. Ke, X. Wei and S. Wang, *Chem.–Asian J.*, 2018, **13**, 3222–3230.
224 H. J. Choi and S. B. Hong, *Chem. Eng. J.*, 2022, **433**, 133800.
225 F. Gholipour and M. Mofarahi, *J. Supercrit. Fluids*, 2016, **111**, 47–54.
226 C. L. Xue, W. P. Cheng, W. M. Hao, J. H. Ma and R. F. Li, *J. Mater. Chem.*, 2019, **2019**, 1–9.
227 H. Moradi, H. Azizpour, H. Bahmanyar, N. Rezamandi and P. Zahedi, *Chem. Eng. Technol.*, 2021, **44**, 1221–1226.
228 D. Knappe and A. R. Campos, *Water Sci. Technol.: Water Supply*, 2005, **5**, 83–91.
229 R. Gonzalez-Olmos, F. D. Kopinke, K. Mackenzie and A. Georgi, *Environ. Sci. Technol.*, 2013, **47**, 2353–2360.
230 D. J. de Ridder, J. Q. J. C. Verberk, S. G. J. Heijman, G. L. Amy and J. C. van Dijk, *Sep. Purif. Technol.*, 2012, **89**, 71–77.
231 Z. L. Cheng, Y. X. Li and Z. Liu, *Ecotoxicol. Environ. Saf.*, 2018, **148**, 585–592.
232 N. Jiang, M. Erdős, O. A. Moultos, R. Shang, T. J. H. Vlugt, S. G. J. Heijman and L. C. Rietveld, *Chem. Eng. J.*, 2020, **389**, 123968.
233 N. Jiang, R. Shang, S. G. J. Heijman and L. C. Rietveld, *Sep. Purif. Technol.*, 2020, **235**, 116152.
234 V. B. Kazansky, V. Y. Borovkov, A. Serich and H. G. Karge, *Microporous Mesoporous Mater.*, 1998, **22**, 251–259.
235 S. H. Jhung, J. W. Yoon, J. S. Lee and J. S. Chang, *Chemistry*, 2007, **13**, 6502–6507.
236 Y. Li and R. T. Yang, *J. Phys. Chem. B*, 2006, **110**, 17175–17181.
237 I. Bezverkhyy, Q. Pujol, C. Dirand, F. Herbst, M. Macaud and J.-P. Bellat, *Microporous Mesoporous Mater.*, 2020, **302**, 110217.
238 M. Kuronen, M. Weller, R. Townsend and R. Harjula, *React. Funct. Polym.*, 2006, **66**, 1350–1361.
239 B. Azambre, M. Chebbi and A. Hijazi, *Chem. Eng. J.*, 2020, **379**, 122308.
240 A. A. Ismail, R. M. Mohamed, I. A. Ibrahim, G. Kini and B. Koopman, *Colloids Surf., A*, 2010, **366**, 80–87.
241 A. Dyer and T. I. Emms, *J. Mater. Chem.*, 2005, **15**, 5012–5021.
242 M. Kuronen, R. Harjula, J. Jernström, M. Vestenius and J. Lehto, *Phys. Chem. Chem. Phys.*, 2000, **2**, 2655–2659.
243 Y. Wang, F. Lin and W. Pang, *J. Hazard. Mater.*, 2008, **160**, 371–375.
244 Z. Wang, W. Chu, Z. Zhao, Z. Liu, H. Chen, D. Xiao, K. Gong, F. Li, X. Li and G. Hou, *J. Phys. Chem. Lett.*, 2021, **12**, 9398–9406.
245 Y. Wang, X. He, F. Yang, Z. Su and X. Zhu, *Ind. Eng. Chem. Res.*, 2020, **59**, 13420–13427.
246 S. Wang, L. Zhang, S. Li, Z. Qin, D. Shi, S. He, K. Yuan, P. Wang, T.-S. Zhao, S. Fan, M. Dong, J. Li, W. Fan and J. Wang, *J. Catal.*, 2019, **377**, 81–97.
247 Y. G. Hur, P. M. Kester, C. T. Nimlos, Y. Cho, J. T. Miller and R. Gounder, *Ind. Eng. Chem. Res.*, 2019, **58**, 11849–11860.
248 J. Dedecek, E. Tabor and S. Sklenak, *ChemSusChem*, 2019, **12**, 556–576.
249 J. Dedecek, M. J. Lucero, C. Li, F. Gao, P. Klein, M. Urbanova, Z. Tvaruzkova, P. Sazama and S. Sklenak, *J. Phys. Chem. C*, 2011, **115**, 11056–11064.

250 A. Janda and A. T. Bell, *J. Am. Chem. Soc.*, 2013, **135**, 19193–19207.
251 D. Barthomeuf, *J. Phys. Chem.*, 1993, **97**, 10092–10096.
252 P. Sazama, E. Tabor, P. Klein, B. Wichterlova, S. Sklenak, L. Mokrzycki, V. Pashkkova, M. Ogura and J. Dedecek, *J. Catal.*, 2016, **333**, 102–114.
253 K. Mlekodaj, J. Dedecek, V. Pashkova, E. Tabor, P. Klein, M. Urbanova, R. Karcz, P. Sazama, S. R. Whittleton, H. M. Thomas, A. V. Fishchuk and S. Sklenak, *J. Phys. Chem. C*, 2019, **123**, 7968–7987.
254 V. Gabova, J. Dedecek and J. Cejka, *Chem. Commun.*, 2003, 1196–1197, DOI: **10.1039/b301634j**.
255 J. Dedecek, S. Sklenak, C. Li, B. Wichterlová, V. Gábová, J. i. Brus, M. Sierka and J. Sauer, *J. Phys. Chem. C*, 2009, **113**, 1447–1458.
256 J. Dědeček, D. Kaucký and B. Wichterlová, *Chem. Commun.*, 2001, 970–971, DOI: **10.1039/b009589n**.
257 N. Wang, M. Zhang and Y. Yu, *Microporous Mesoporous Mater.*, 2013, **169**, 47–53.
258 J. Dedecek, V. Balgová, V. Pashkova, P. Klein and B. Wichterlová, *Chem. Mater.*, 2012, **24**, 3231–3239.
259 T. Yokoi, H. Mochizuki, S. Namba, J. N. Kondo and T. Tatsumi, *J. Phys. Chem. C*, 2015, **119**, 15303–15315.
260 T. Biligetu, Y. Wang, T. Nishitoba, R. Otomo, S. Park, H. Mochizuki, J. N. Kondo, T. Tatsumi and T. Yokoi, *J. Catal.*, 2017, **353**, 1–10.
261 T. Yokoi, H. Mochizuki, T. Biligetu, Y. Wang and T. Tatsumi, *Chem. Lett.*, 2017, **46**, 798–800.
262 A. B. Pinar, L. Gómez-Hortigüela, L. B. McCusker and J. Pérez-Pariente, *Chem. Mater.*, 2013, **25**, 3654–3661.
263 K. Muraoka, W. Chaikittisilp, Y. Yanaba, T. Yoshikawa and T. Okubo, *Angew. Chem., Int. Ed.*, 2018, **57**, 3742–3746.
264 H. Jongkind, K. Datema, S. Nabuurs, A. Seive and W. Stork, *Microporous Mater.*, 1997, **10**, 149–161.
265 M. Liu, T. Yokoi, M. Yoshioka, H. Imai, J. N. Kondo and T. Tatsumi, *Phys. Chem. Chem. Phys.*, 2014, **16**, 4155–4164.
266 W. Lv, S. Wang, P. Wang, Y. Liu, Z. Huang, J. Li, M. Dong, J. Wang and W. Fan, *J. Catal.*, 2021, **393**, 190–201.
267 J. R. Di Iorio, S. Li, C. B. Jones, C. T. Nimlos, Y. Wang, E. Kunkes, V. Vattipalli, S. Prasad, A. Moini, W. F. Schneider and R. Gounder, *J. Am. Chem. Soc.*, 2020, **142**, 4807–4819.
268 J. Chen, T. Liang, J. Li, S. Wang, Z. Qin, P. Wang, L. Huang, W. Fan and J. Wang, *ACS Catal.*, 2016, **6**, 2299–2313.
269 C. Li, A. Vidal-Moya, P. J. Miguel, J. Dedecek, M. Boronat and A. Corma, *ACS Catal.*, 2018, **8**, 7688–7697.
270 K. Chen, X. Wu, J. Zhao, H. Zhao, A. Li, Q. Zhang, T. Xia, P. Liu, B. Meng, W. Song, X. Zhu, H. Liu, X. Gao, C. Xu and B. Shen, *J. Catal.*, 2022, **413**, 735–750.
271 P. Sazama, J. Dedecek, V. Gabova, B. Wichterlova, G. Spoto and S. Bordiga, *J. Catal.*, 2008, **254**, 180–189.
272 J. Devos, M. L. Bols, D. Plessers, C. V. Goethem, J. W. Seo, S.-J. Hwang, B. F. Sels and M. Dusselier, *Chem. Mater.*, 2019, **32**, 273–285.
273 T. Nishitoba, N. Yoshida, J. N. Kondo and T. Yokoi, *Ind. Eng. Chem. Res.*, 2018, **57**, 3914–3922.
274 M. Yabushita, Y. Imanishi, T. Xiao, R. Osuga, T. Nishitoba, S. Maki, K. Kanie, W. Cao, T. Yokoi and A. Muramatsu, *Chem. Commun.*, 2021, **57**, 13301–13304.
275 K. Yuan, X. Jia, S. Wang, S. Fan, S. He, P. Wang, Z. Qin, M. Dong, W. Fan and J. Wang, *Microporous Mesoporous Mater.*, 2022, **341**, 112051.
276 E. Hoseinynezhad and F. Varaminian, *J. Mol. Liq.*, 2019, **292**, 111279.
277 A. Vjunov, J. L. Fulton, T. Huthwelker, S. Pin, D. Mei, G. K. Schenter, N. Govind, D. M. Camaioni, J. Z. Hu and J. A. Lercher, *J. Am. Chem. Soc.*, 2014, **136**, 8296–8306.
278 J. Holzinger, P. Beato, L. F. Lundegaard and J. Skibsted, *J. Phys. Chem. C*, 2018, **122**, 15595–15613.
279 M. Haouas, F. Taulelle and C. Martineau, *Prog. Nucl. Magn. Reson. Spectrosc.*, 2016, **94–95**, 11–36.
280 M. Gackowski, J. Podobinski, E. Broclawik and J. Datka, *Molecules*, 2019, **25**, 31.
281 Z. J. Berkson, M. F. Hsieh, S. Smeets, D. Gajan, A. Lund, A. Lesage, D. Xie, S. I. Zones, L. B. McCusker, C. Baerlocher and B. F. Chmelka, *Angew. Chem., Int. Ed.*, 2019, **58**, 6255–6259.
282 C. Martineau-Corcos, J. Dedecek and F. Taulelle, *Solid State Nucl. Magn. Reson.*, 2017, **84**, 65–72.
283 S. Sklenak, J. Dedecek, C. Li, B. Wichterlova, V. Gabova, M. Sierka and J. Sauer, *Angew. Chem., Int. Ed.*, 2007, **46**, 7286–7289.
284 E. Dib, T. Mineva, E. Veron, V. Sarou-Kanian, F. Fayon and B. Alonso, *J. Phys. Chem. Lett.*, 2018, **9**, 19–24.
285 A. B. Pinar, P. Rzepka, A. J. Knorpp, L. B. McCusker, C. Baerlocher, T. Huthwelker and J. A. van Bokhoven, *J. Am. Chem. Soc.*, 2021, **143**, 17926–17930.
286 J. E. Schmidt, L. Peng, J. D. Poplawsky and B. M. Weckhuysen, *Angew. Chem., Int. Ed.*, 2018, **57**, 10422–10435.
287 B. Gault, A. Chiaramonti, O. Cojocaru-Mirédin, P. Stender, R. Dubosq, C. Freysoldt, S. K. Makineni, T. Li, M. Moody and J. M. Cairney, *Nat. Rev. Methods Primers*, 2021, **1**, 1–30.
288 D. E. Perea, I. Arslan, J. Liu, Z. Ristanovic, L. Kovarik, B. W. Arey, J. A. Lercher, S. R. Bare and B. M. Weckhuysen, *Nat. Commun.*, 2015, **6**, 7589.
289 J. E. Schmidt, J. D. Poplawsky, B. Mazumder, O. Attila, D. Fu, D. A. de Winter, F. Meirer, S. R. Bare and B. M. Weckhuysen, *Angew. Chem., Int. Ed.*, 2016, **55**, 11173–11177.
290 A. V. Yakimov, V. L. Sushkevich, J. A. van Bokhoven and C. Copéret, *J. Phys. Chem. C*, 2022, **126**, 3681–3687.
291 H. Toyoda, R. Osuga, Y. Wang, S. Park, K. Yazawa, H. Gies, C. J. Gilbert, B. Yilmaz, C. P. Kelkar and T. Yokoi, *Phys. Chem. Chem. Phys.*, 2022, **24**, 4358–4365.
292 J. Dědeček, D. Kaucký, B. Wichterlová and O. Gonsiorová, *Phys. Chem. Chem. Phys.*, 2002, **4**, 5406–5413.
293 E. E. Bickel, C. T. Nimlos and R. Gounder, *J. Catal.*, 2021, **399**, 75–85.
294 L. Liu, N. Wang, C. Zhu, X. Liu, Y. Zhu, P. Guo, L. Alfilfil, X. Dong, D. Zhang and Y. Han, *Angew. Chem., Int. Ed.*, 2020, **59**, 819–825.

295 J. M. Findley, P. I. Ravikovitch and D. S. Sholl, *J. Phys. Chem. C*, 2018, **122**, 12332–12340.
296 S. Park, T. Biligetu, Y. Wang, T. Nishitoba, J. N. Kondo and T. Yokoi, *Catal. Today*, 2018, **303**, 64–70.
297 A. A. C. Reule, J. A. Sawada and N. Semagina, *J. Catal.*, 2017, **349**, 98–109.
298 L. Zhang, S. Wang, D. Shi, Z. Qin, P. Wang, G. Wang, J. Li, M. Dong, W. Fan and J. Wang, *Catal. Sci. Technol.*, 2020, **10**, 1835–1847.
299 A. J. Hoffman, J. S. Bates, J. R. Di Iorio, S. V. Nystrom, C. T. Nimlos, R. Gounder and D. Hibbitts, *Angew. Chem., Int. Ed.*, 2020, **59**, 18686–18694.
300 Z. Liu, T. Wakihara, K. Oshima, D. Nishioka, Y. Hotta, S. P. Elangovan, Y. Yanaba, T. Yoshikawa, W. Chaikittisilp, T. Matsuo, T. Takewaki and T. Okubo, *Angew. Chem., Int. Ed.*, 2015, **54**, 5683–5687.
301 W. Lv, P. Meng, Z. Qin, J. Li, M. Dong, J. Wang and W. Fan, *Microporous Mesoporous Mater.*, 2021, **313**, 110851.
302 L. Chen, H. Falsig, T. V. W. Janssens, J. Jansson, M. Skoglundh and H. Grönbeck, *Catal. Sci. Technol.*, 2018, **8**, 2131–2136.
303 H. V. Thang, L. Grajciar, P. Nachtigall, O. Bludský, C. O. Areán, E. Frýdová and R. Bulánek, *Catal. Today*, 2014, **227**, 50–56.
304 E. Dempsey, G. Kühl and D. H. Olson, *J. Phys. Chem.*, 1969, **73**, 387–390.
305 C.-T. Yang, A. Janda, A. T. Bell and L.-C. Lin, *J. Phys. Chem. C*, 2018, **122**, 9397–9410.
306 D. Schwalbe-Koda, S. Kwon, C. Paris, E. Bello-Jurado, Z. Jensen, E. Olivetti, T. Willhammar, A. Corma, Y. Román-Leshkov and M. Moliner, *Science*, 2021, **374**, 308–315.
307 J. Jiang, Y. Xu, P. Cheng, Q. Sun, J. Yu, A. Corma and R. Xu, *Chem. Mater.*, 2011, **23**, 4709–4715.
308 Y. Li, C. Shi, L. Li, G. Yang, J. Li, J. Xu, Q. Gu, X. Wang, J. Han, T. Zhang, Y. Li and J. Yu, *Natl. Sci. Rev.*, 2022, **9**, nwac094.
309 M. Moliner, Y. Roman-Leshkov and A. Corma, *Acc. Chem. Res.*, 2019, **52**, 2971–2980.